UNIVERSITY OF HELSINKI REPORT SERIES IN PHYSICS

HU-P-D136

DYNAMICS OF FREE-RUNNING, PUMP-MODULATED AND COUPLED SEMICONDUCTOR AND SOLID-STATE LASERS

Thomas Fordell

Accelerator Laboratory
Department of Physical Sciences
Faculty of Science
University of Helsinki
Helsinki, Finland

ACADEMIC DISSERTATION

To be presented, with the permission of the Faculty of Science of the University of Helsinki, for public criticism in Auditorium D101 of Physicum on 13th April 2007, at 13 o'clock.

Helsinki 2007

ISBN 978-952-10-3237-0 (printed version)
ISSN 0356-0961
Helsinki 2007
Helsinki University Printing House (Yliopistopaino)

ISBN 978-952-10-3238-7 (PDF version)
http://ethesis.helsinki.fi/
Helsinki 2007
Electronic Publications @ University of Helsinki (Helsingin yliopiston verkko-julkaisut)

T. Fordell: Dynamics of free-running, pump-modulated and coupled semiconductor and solid-state lasers, University of Helsinki, 2007, 81 pages + appendices.
University of Helsinki Report Series in Physics, HU-P-D136, ISSN 0356-0961, ISBN 978-952-10-3237-0 (printed version), ISBN 978-952-10-3238-7 (PDF version).

Classification (INSPEC): A4255P, A4255Q, A4265T
Keywords (INSPEC): Semiconductor lasers, microchip lasers, nonlinear dynamical systems

ABSTRACT

The output of a laser is a propagating electromagnetic field with superior coherence and brightness compared to that emitted by thermal sources. A multitude of different types of lasers exist, which also translates into large differences in the properties of their output. Moreover, the characteristics of the electromagnetic field emitted by a laser can be influenced from the outside, e.g., by injecting an external optical field or by optical feedback.

In the case of free-running solitary class-B lasers, such as semiconductor and Nd:YVO_4 solid-state lasers, the phase space is two-dimensional, the degrees of freedom being the population inversion and the amplitude of the electromagnetic field. The two-dimensional structure of the phase space means that no complex dynamics can be found. If a class-B laser is perturbed from its steady state, then the steady state is restored after a short transient. However, as discussed in part (i) of this Thesis, the static properties of class-B lasers, as well as their artificially or noise induced dynamics around the steady state, can be experimentally studied in order to gain insight on laser behaviour, and to determine model parameters that are not known ab initio. In this Thesis particular attention is given to the linewidth enhancement factor, which describes the coupling between the gain and the refractive index in the active material.

A highly desirable attribute of an oscillator is stability, both in frequency and amplitude. Nowadays, however, instabilities in coupled lasers have become an active area of research motivated not only by the interesting complex nonlinear dynamics but also by potential applications. In part (ii) of this Thesis the complex dynamics of unidirectionally coupled, i.e., optically injected, class-B lasers is investigated. An injected optical field increases the dimensionality of the phase space to three by turning the phase of the electromagnetic field into an important variable. This has a radical effect on laser behaviour, since very complex dynamics, including chaos, can be found in a nonlinear system with three degrees of freedom. The output of the injected laser can be controlled in experiments by varying the injection rate and the frequency of the injected light. In this Thesis the dynamics of unidirectionally coupled semiconductor and Nd:YVO_4 solid-state lasers is studied numerically and experimentally.

CONTENTS

Abstract i

Structure and List of Articles 1

1. Background 5

1.1 Semiconductor Lasers 6

1.2 Nd:YVO_4 Solid-State Lasers 9

1.3 Classification 10

2. Modelling 13

2.1 The Laser Model 13

2.2 The Steady State 19

2.3 Dynamics 21

2.4 Noise 22

2.5 Pump Modulation 26

3. Coupled Oscillators 31

3.1 Coupled Class-B Lasers 32

4. Optically Injected Lasers 35

4.1 Small-Signal Regime 36

4.2 Large-Signal Regime 38

5. Optical Injection Experiments 49
5.1 Semiconductor Lasers 50
5.2 Nd:YVO_4 Solid-State Lasers 51
5.3 Applications 53

6. Concluding Remarks 59
6.1 Outlook 60

Errata 62

Acknowledgements 63

Bibliography 65

STRUCTURE AND LIST OF ARTICLES

This Thesis consists of an introduction and five articles published in international peer-reviewed scientific journals. The articles will be referred to by bold face roman numerals in the main text.

In writing the six introductory chapters, the author has tried to write an introduction to the subject of this Thesis while avoiding, as much as possible, the more detailed contents of the publications. Also, the author has tried to put his work into a historical context – from the invention of lasers and the relevant physics in the first chapter to the contemporary and potential future applications presented in Chapter 5 which utilise the various properties of coupled lasers discussed in the preceding chapters.

The introduction is organised as follows. Part (i), which includes Chapters 1 and 2, discusses the properties of solitary free-running and pump-modulated lasers. Chapter 1 gives a short review of the historical milestones that led to masers and to the contemporary semiconductor and Nd:YVO_4 microchip solid-state lasers studied in articles **I-V**. In Chapter 2 basic laser properties are reviewed with the help of a rate-equation model, including steady-state solutions, noise properties and modulation response. Whenever appropriate, model and laser properties are demonstrated with examples from the articles.

Part (ii) of the introduction, i.e., Chapters 3-5, discusses the dynamics of unidirectionally coupled lasers, which differs from that of solitary lasers due to the increased dimensionality of the phase space. Chapter 3 turns the focus from solitary lasers towards coupled oscillators, starting with a brief historical background. In Chapter 4 the rate-equation model introduced in Chapter 2 is complemented with an injected optical field. Analytical solutions in the small signal regime are given as well as different numerical approaches that can be utilised in the large signal regime, where the injected field can no longer be treated as a perturbation. In Chapter 5 experiments on unidirectionally coupled semiconductor lasers and Nd:YVO_4 microchip solid-state lasers are presented and compared with numerical results. Chapter 5 is concluded by presenting contemporary and potential future applications where the various dynamical states discussed in Chapters 3-5 can be used to advantage. Concluding remarks are given in Chapter 6. The original scientific articles, the abstracts of which are given on the next two pages, are reproduced in the appendices with permission from the publishers.

Abstracts of the original articles

I: T. Fordell and Å.M. Lindberg, "Experiments on the linewidth enhancement factor of a vertical-cavity surface-emitting laser", *Journal of Quantum Electronics*, vol. 43, no. 1, pp. 6-15, 2007

Nine different experimental techniques for measuring the linewidth enhancement factor α are discussed and tested on a single 760-nm vertical-cavity surface-emitting laser. Techniques included in the comparison are based on linewidth measurements, current modulation, optical injection and optical feedback.

II: T. Fordell, Z. Toffano and Å.M. Lindberg, "A vertical-cavity surface-emitting laser at threshold", *Photonics Technology Letters*, vol. 18, no. 21, pp. 2263-2265, 2006

Linewidth is measured over the threshold transition of a vertical-cavity surface-emitting laser and results are compared to a Fokker-Planck semiconductor laser model. The linewidth shows nonmonotonous behaviour at threshold similar to that previously observed in distributed feedback lasers. The behaviour agrees with the Fokker-Planck model if the linewidth enhancement factor $\alpha \approx 5.0$. Measurement of the relaxation oscillation frequency and the damping rate using an injected optical probe allows, together with the Fokker-Planck model, the extraction of major laser parameters.

III: T. Fordell, S. Valling and Å.M. Lindberg, "Modulation and the linewidth enhancement factor of a diode-pumped Nd:YVO_4 laser", *Optics Letters*, vol. 30, no. 22, pp. 3036-3038, 2005

A technique based on an FM/AM method is proposed for measuring the linewidth enhancement factor α of a diode-pumped Nd:YVO_4 laser. A standard rate equation model is complemented with temperature effects to explain the observed behavior under pump modulation. The result $\alpha = 0.25 \pm 0.13$ agrees with values deduced from recent optical injection experiments.

IV: S. Valling, T. Fordell and Å.M. Lindberg, "Maps of the dynamics of an optically injected solid-state laser", *Physical Review A*, vol 72, 033810, 2005

Maps of the dynamics of an optically injected solid-state Nd:YVO_4 laser are presented. Experimental maps showing different dynamical regions are generated automatically from measured intensity time series by plotting the maxima of intensity. Corresponding numerical maps and a bifurcation diagram are calculated with a rate equation model of an injected class B laser. Intensity time series inside different regions in the maps are examined. The experimental and numerical maps are shown to be in good agreement with each other if the linewidth enhancement factor α is used as a fitting parameter in the model. As a result, experimental estimates for an effective α are given for a Nd:YVO_4 laser. The effects of noise on the dynamics are also discussed.

V: T. Fordell and Å.M. Lindberg, "Numerical stability maps of an optically injected semiconductor laser", *Optics Communications*, vol 242, no. 4-6, pp. 613-622, 2004

Detailed experimental mappings of the dynamics of a Fabry-Pérot type semiconductor laser subjected to external optical injection along with parameters describing the injected laser have been published by Eriksson and Lindberg [J. Opt. B: Quantum Semiclass. Opt. 4 (2002) 149] and by Eriksson [Opt. Commun. 210 (2002) 343]. This paper reports on a numerical investigation of the injection experiments. By computing the largest Lyapunov exponent, the chaotic islands, periodic windows and locking ranges are compared in detail with the experimental results for three different operating points of the laser. The numerical results are in good agreement with the experiment once the linewidth enhancement factor is increased from the earlier reported value of 3.9 ± 0.5 to about 6.7. The new value is confirmed by a re-measurement of the linewidth enhancement factor using a current modulation technique.

Author's contribution

I: All experiments and modelling were performed by the author. The paper was written by the author of this Thesis.

II: The author performed the measurements and wrote the article. Modelling was done by Prof. Zeno Toffano, Supélec (Ecole Supérieure d'Electricité), France.

III: The author developed the experimental procedure, performed the data analysis and modelling, and took part in the experiments. The paper was written by the author of this Thesis.

IV: The experimental procedure for mapping the dynamics was conceived by the author, who also wrote the computer programs used for modelling and devised the parameter extraction procedure. A minor part of the paper (most of Section III) was written by the author of this Thesis.

V: The author performed the computer modelling and the measurements. The paper was written by the author of this Thesis.

1. BACKGROUND

Lasers are oscillators that operate at frequencies corresponding to the ultra-violet, visible and infrared parts of the electromagnetic spectrum. In general, an oscillator consists of two parts: a feedback network that provides positive feedback and an active part that provides amplification. The physics that allows lasers to be constructed was discovered in the beginning of the 20th century, and the technical foundation was laid in the 1950s.

In 1900, M. Planck managed to derive an expression for black-body radiation, which was, in contrast to Wien's law, in remarkable agreement with measurements [1]. In his derivation, Planck introduced the concept of energy quantisation, but he used it only as a formal assumption, a mathematical hypothesis, without emphasising the discrete nature of real energy-exchange processes. Later, in 1917, A. Einstein considered atoms in thermal equilibrium with a radiation field and demonstrated that, in order to obtain the correct energy density formula derived by Planck for black-body radiation, stimulated emission of radiation from excited atoms must be taken into account [2-4]. In stimulated emission, a photon, a quantum of the electromagnetic field, stimulates a downward transition of an excited atom. Additionally, Einstein predicted that the photon is emitted in the same direction as the stimulating photon is travelling in. However, Einstein did not consider coherence. Although a proof of coherence was lacking, the coherence property of stimulated emission was recognised by many physicists working in the field in the 1920s and 1930s [5]. Stimulated emission, therefore, leads to coherent amplification of electromagnetic fields and allows oscillators operating at optical frequencies to be constructed. It took, however, another three decades until the vital technical discoveries were made.

In thermal equilibrium there are more electrons in the lower energy levels than in the higher ones. As a consequence, incoming radiation will, on average, stimulate more upward transitions than downward, which results in net absorption of radiation. Efforts to figure out ways of producing millimetre waves for applications such as radars and microwave communications systems led C.H. Townes in 1951 to make the final and crucial discovery. Townes realised that the constituent species of an amplifier do not have to be in thermal equilibrium. If the atoms, or molecules, are prepared with a population inversion, which was routinely done in various laboratories at that time, and enclosed in a resonator, then

net amplification of the electromagnetic field inside the resonator would result.

The first working device, a maser (microwave amplification by stimulated emission of radiation), was constructed at Columbia University in 1954. It consisted of a hollow metal cylinder as the feedback element and a beam of excited ammonia molecules that provided amplification of the electromagnetic field. The energy levels employed were two vibrational states of the ammonia molecule with an energy difference corresponding to 23.87 GHz.

Concurrently, in the Soviet Union, A. Prokhorov and N. Basov did work on microwaves independently of the Americans. In 1954 they published a theoretical paper describing a similar maser concept, and later, they were the first to produce a continuous wave (CW) maser by utilising more than two energy levels.

The success of masers drew attention towards oscillators at even shorter wavelengths. A. Schawlow and C.H. Townes were the first to publish detailed calculations on how to construct optical masers [6]. These devices were later dubbed lasers (light amplification by stimulated emission of radiation). Lasing at optical frequencies was first demonstrated by T. Maiman in 1960 [7]. He used a flash-lamp-pumped ruby crystal and achieved pulsed lasing at 694 nm. By the end of the same year, lasing at infrared or visible wavelengths had been demonstrated in five different devices [8], including the first CW infrared laser, the He-Ne gas laser, by A. Javan *et al.* [9].

1.1 Semiconductor Lasers

J. von Neumann is believed to be the first to consider theoretically light amplification in a pn-junction in 1953 although his results remained unpublished [10]. During the late 1950s and early 1960s many scientist worked independently on the problem, and their efforts led to the demonstration of laser operation by four different groups in 1962 (for references see [10]). The first devices were homostructure devices, meaning that the same semiconductor material was used throughout the active region; only the doping was varied. These devices had high current thresholds even at cryogenic temperatures and were capable of only pulsed operation. The heterostructure and double-heterostructure configurations were invented a year later and a suitable lattice matched AlGaAs-GaAs system was discovered in 1967 [11]. In a double-heterostructure laser a low band-gap material is sandwiched between two high band-gap materials (Fig. 1.1). Such an arrangement improves electron and hole confinement, reduces absorption away from the active region, and provides wave guiding due to the varying refractive index. Progress was rapid after these important breakthroughs. Room temperature CW operation of a semiconductor laser was demonstrated in 1970 independently by Z. Alferov in the Soviet Union and by I. Hayashi and M. Panish at Bell Telephone Laboratories in the United States.

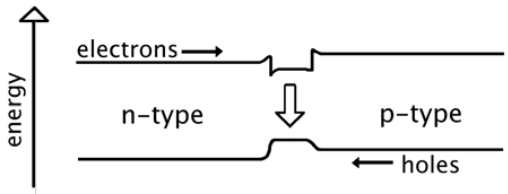

Fig. 1.1: Schematic band diagram of a double-heterostructure semiconductor laser under forward bias. (Note that the detailed band structure depends on the materials and doping levels.)

The efficiency of heterostructure junctions can be further improved by making the active region very thin so that quantum effects come into play. In quantum-well, quantum-wire and quantum-dot structures the density of states function is such that the electrons are concentrated into states that contribute to light amplification. Most commercial devices of today, also those used in this Thesis, have active regions consisting of several quantum wells.

The hallmark of a pn-junction is its ability to rectify currents. Very little current flows through the junction in the backward direction, but in the forward direction current increases exponentially with applied voltage. This sensitivity to the applied voltage in the forward direction means that, in order to keep the supply of carriers to the active region constant, diode lasers must be pumped by current sources rather than voltage sources. The voltage, which also depends on the temperature and the carrier density, is free to drift.

The oscillation frequency of lasers is sensitive to the cavity temperature. Therefore, active temperature control circuitry is needed in most experiments, also in those reported on here. Although not used in this work, improved frequency stability in free-running lasers, compared to that achievable with traditional temperature control circuitry, can be obtained by monitoring the junction voltage and feeding this signal back to the temperature controller [12, 13, 14].

1.1.1 Edge-Emitting Lasers

Conventional semiconductor lasers are edge-emitting Fabry-Pérot (FP) devices (Fig. 1.2). In these lasers the active region is parallel to the cavity, which means that the gain per round trip is very high. Consequently, lasing can be achieved even with naturally cleaved crystal facets as mirrors. The single-mode properties of small devices can be significantly improved by incorporating a distributed feedback (DFB) structure into the laser cavity. Moreover, optical feedback from an external mirror or a grating can reduce the linewidth from the MHz level to the 100 kHz level and below.

Typical output characteristics of contemporary commercial (small) devices are

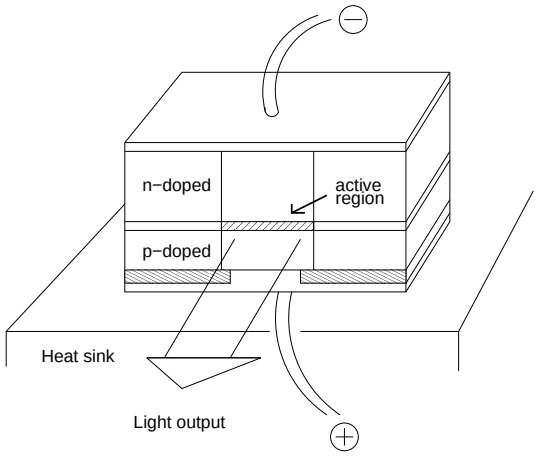

Fig. 1.2: A schematic of a basic index guided edge-emitting semiconductor laser. A multitude of different cavity designs exist.

10-100 milliwatts of output power with threshold currents of a few tens of milliamperes. These lasers are used in laser pointers, CD and DVD players, interferometry, spectroscopy and optical fibre communications. High-power broad-area edge-emitting lasers (EELs) produce several watts of output power with poor beam quality. Such devices are often used to optically pump solid-state lasers.

1.1.2 Vertical-Cavity Surface-Emitting Lasers

Lasing orthogonally to the substrate surface and in the longitudinal direction with respect to the current was first reported by I. Melngailis in 1965 [15]. His InSb surface-emitting laser (SEL) operated only in pulsed mode at liquid nitrogen temperatures and required a strong external magnetic field to confine the carriers. The most successful SEL is the vertical-cavity surface-emitting laser (VCSEL), where the active layer is perpendicular to the cavity. The VCSEL concept was proposed by K. Iga in 1977. VCSEL cavities consist of an active region, e.g., a multi-quantum-well structure, sandwiched between high reflectivity planar distributed Bragg reflector (DBR) mirrors. The first working VCSEL was demonstrated in 1979 by H. Soda *et al.* [16]. It operated in pulsed mode at liquid nitrogen temperatures at 1300 nm. A decade later, in 1988, CW room-temperature operation was achieved by F. Koyama *et al.* at 890 nm [17].

VCSELs exhibit many desirable features, including low threshold current, dynamic single-mode operation, circular output beam, and reduced sensitivity to feedback. Many more features are listed in [18]. Less attractive features include low output power in single-mode devices and polarisation instabilities, particularly in older devices. In order to suppress higher order transverse modes, the lateral dimensions of single-mode devices must be kept small. Small dimensions

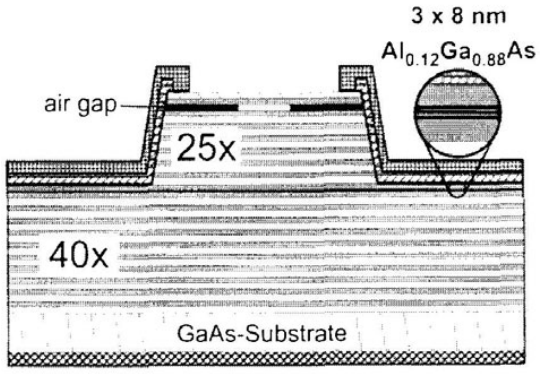

Fig. 1.3: A schematic of a VCSEL. The VCSEL studied in articles **I** and **II** has a similar structure but it lacks an air gap for current confinement. Doping levels are also different. This Figure has been reprinted from [20] with permission from the publisher.

mean low output powers. Polarisation switching has been widely studied both from a dynamical systems point of view and from a device manufacturing point of view. By including symmetry breaking features in the cavity, the polarisation switching can be eliminated. The state-of-the-art in VCSEL technology include 60-nm micro-electro-mechanically (MEMS) tunable VCSELs [19], threshold currents in the μA region, and 10 mW of single-mode output power (not all in the same devices though).

The structure of the commercial air-post VCSEL studied in articles **I** and **II** of this Thesis is shown in Fig. 1.3. The lasers consist of 25 periods of $Al_{0.38}GaAs/AlAs$ quarter-wave layers in the top (p-doped) and 40 periods (n-doped) in the bottom Bragg reflector. The 1-λ $Al_{0.4}GaAs$ cavity incorporates three 8-nm $Al_{0.14}GaAs$ quantum wells designed for 760-nm operation [21]. The threshold current is 2.90 mA at room temperature, and the maximum output power is just below 1 mW.

1.2 Nd:YVO_4 Solid-State Lasers

The potential of neodymium-doped yttrium orthovanadate (Nd:YVO_4) as a laser material was recognised already in the mid 1960s [22]. Development of laser systems based on this crystal was hindered by the difficulty in growing large high-quality crystals suitable for flash-lamp pumping. Improvements in crystal growth processes and the availability of semiconductor lasers for efficient pumping has made Nd:YVO_4 crystals one of the most efficient gain media available for diode-pumped solid-state lasers. It has a large stimulated emission cross-section at 1064 nm, a high pump-absorption coefficient (3.7 mm^{-1} for 1% doping) and a large

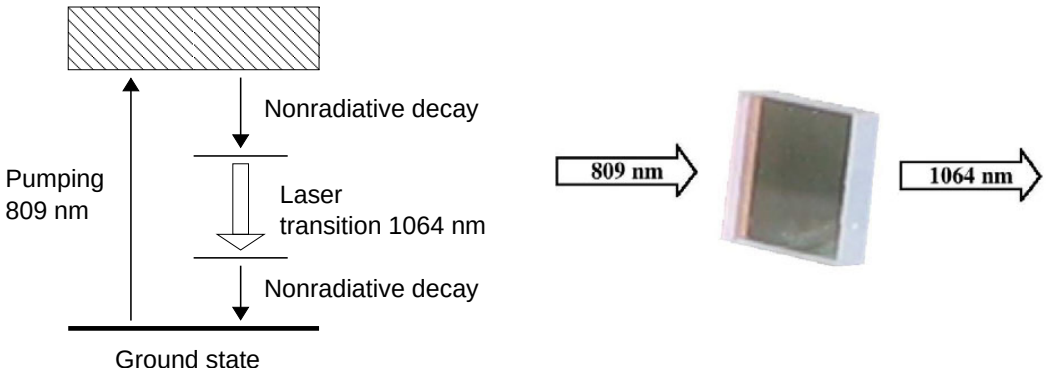

Fig. 1.4: Simplified Nd:YVO_4 energy level diagram (left) and a photograph of a 3x3x1-mm^3 Nd:YVO_4 crystal used in articles **III** and **IV** (right).

pump-absorption bandwidth at 809-nm pump wavelengths (>10 nm).

A simplified energy level diagram is shown on the left in Fig. 1.4. The Nd:YVO_4 laser is a four-level system. Electrons in the dopant Nd atoms are optically excited to high-lying pump levels from which they rapidly decay (< 1 ns) nonradiatively to the upper laser level [23]. The upper laser level lifetime is 90 μs for 1% doping [24]. From the lower laser level electrons decay fast (<1 ns) back to the ground state [25]. Nd:YVO_4 is often considered an ideal four-level laser gain material owing to the five orders of magnitude difference between the upper and lower level lifetimes. In spite of that, the lower level lifetime does play a crucial role when noise and modulation response are considered in Chapter 2.

A photograph of a 3x3x1-mm^3 Nd:YVO_4 crystal used in articles **III** and **IV** is shown on the right in Fig. 1.4. The pump-side facet of the 1-mm thick crystal is coated for very high reflectivity ($R_1 > 99\%$) at 1064 nm and for very low reflectivity at 809 nm. The output facet has a reflection coefficient of $R_2 = 95\%$ at 1064 nm.

1.3 Classification

From a dynamics point of view it is convenient to classify lasers not by their construction, but by their degrees of freedom [26, 27]. Single-mode lasers can be described by three autonomous first-order differential equations – one for the slowly varying complex amplitude of the electromagnetic (EM) field, one for the slowly varying complex material polarisation, and one for the population inversion. The relative magnitudes of the damping rates of these three quantities play a fundamental role in the type of behaviour displayed by lasers.

In class-A lasers, e.g., dye lasers, the population and the material polarisation relax much faster than the EM field. Before the EM field has time to change,

the population and the material polarisation will have decayed to their steady-state values and can, therefore, be adiabatically eliminated, i.e., replaced by their steady-state values. This adiabatic elimination reduces the dimensionality of the system of equations to just one. Hence, only fixed-point (steady-state) solutions can exist.

In class-B lasers, e.g., semiconductor and Nd:YVO_4 solid-state lasers, only the material polarisation can be adiabatically eliminated. The system of equations is thus three dimensional. However, as will be shown in the next chapter, the phase of the EM field decouples and what is left is a system of equations with only two degrees of freedom – the slowly varying amplitude of the electric field and the population inversion. In a two-dimensional autonomous system only constant or periodic solutions exist.

Finally, in class-C lasers, all the variables relax on similar time scales and none of them can be adiabatically eliminated. In a nonlinear system with at least three degrees of freedom very complex dynamics is allowed, including quasi-periodicity and chaos. In 1975 H. Haken [28, 29] demonstrated that, in the case of resonant tuning, the laser rate equations are isomorphic to the Lorenz model for atmospheric convection [30], which was known to exhibit chaotic dynamics. The onset of instabilities in free-running single-mode class-C lasers requires very high pumping conditions, one exception being the NH_3 far infrared (FIR) laser [31]. In 1984 a period-doubling route to chaos in a single-mode NH_3 laser operating at 81 μm was demonstrated by C. Weiss *et al.* [32, 33].

This work deals exclusively with class-B lasers. In the next chapter a more in-depth look at the properties of such lasers is given.

2. MODELLING

This chapter introduces a simple laser model that has been utilised extensively in this Thesis. With the help of this model basic properties of class-B lasers are reviewed, including steady-state behaviour, noise properties and modulation response.

2.1 The Laser Model

In this Thesis, lasers are described by a phenomenological rate-equation model of single-mode class-B lasers [34, 35]

$$\frac{\mathrm{d}E}{\mathrm{d}t} = -\frac{\gamma_c}{2}E + i(\omega_0 - \omega_c)E + \frac{\Gamma}{2}gE + F_E \tag{2.1}$$

$$\frac{\mathrm{d}N}{\mathrm{d}t} = J - R(N) - \frac{2\epsilon_0 n^2}{\hbar\omega_0}\mathrm{Re}\{g\}|E|^2 + F_N. \tag{2.2}$$

In the equation for the the slowly varying envelope of the electric field E, γ_c is the cavity decay rate, ω_0 is the angular frequency of the optical field of the free-running laser, and ω_c is the cold cavity angular resonance frequency. The confinement factor Γ describes the spatial overlap of the optical field and the (complex) gain rate $g = g' + ig''$. The gain arises due to stimulated emission and is related to the carrier induced susceptibility via

$$g = \frac{i\omega_0}{\epsilon_0 n n_g}\chi \tag{2.3}$$

where n is the refractive index, n_g is the group refractive index, and ϵ_0 is the permittivity of vacuum. Field noise due to spontaneous emission is modelled with the Langevin white noise source F_E

$$\langle F_E(t)F_E^*(t-\tau)\rangle = R_E\delta(\tau) \tag{2.4}$$

where R_E is a constant to be determined.

In the equation for the carrier density[1] N, J is the pump rate[2], $R(N)$ is the carrier recombination rate, and F_N is a Langevin noise source that describes

[1] When solid-state devices are considered, N is the number density of electrons in the upper laser level.

[2] In article **V** the pump-rate of a semiconductor laser is written as $\frac{J}{ed}$ where J is the current

noise in the pump and due to spontaneous emission. Above threshold, the recombination rate $R(N)$ can be expanded into a Taylor series at the operating point

$$\begin{aligned} R(N) &= R(N_0) + \frac{\partial R}{\partial N}(N - N_0) + ... \\ &\simeq R(N_0) - \frac{\partial R}{\partial N}N_0 + \frac{\partial R}{\partial N}N \\ &= R_0 + \gamma_s N \end{aligned} \tag{2.5}$$

where $\gamma_s = \partial R/\partial N$ is the small signal carrier decay rate. Here and below, steady-state values are denoted by a subscript '0' and the derivatives are evaluated at the operating point.

The gain rate $g = g(N, |E|^2)$ is also expanded into a series at the operating point

$$\begin{aligned} g(N, |E|^2) &\simeq g(N_0, |E_0|^2) + (\frac{\partial g'}{\partial N} + i\frac{\partial g''}{\partial N})(N - N_0) \\ &+ (\frac{\partial g'}{\partial |E|^2} + i\frac{\partial g''}{\partial |E|^2})(|E|^2 - |E_0^2|) \\ &= g(N_0, |E_0|^2) \\ &+ (1 - i\alpha)\frac{\partial g'}{\partial N}(N - N_0) + (1 - i\beta)\frac{\partial g'}{\partial |E|^2}(|E|^2 - |E_0|^2). \end{aligned} \tag{2.6}$$

The second term in the above expression is the differential gain and the last term is the nonlinear gain. The linewidth enhancement factor (LEF) α is defined by

$$\alpha = \frac{\partial \chi'/\partial N}{\partial \chi''/\partial N} = -\frac{\partial g''/\partial N}{\partial g'/\partial N} \tag{2.7}$$

and β by

$$\beta = \frac{\partial \chi'/\partial |E|^2}{\partial \chi''/\partial |E|^2} = -\frac{\partial g''/\partial |E|^2}{\partial g'/\partial |E|^2} \tag{2.8}$$

where χ' and χ'' are the real and complex parts of the susceptibility, respectively. The LEF and β are discussed in more detail in the next subsection.

Defining the normalised field amplitude $A = E/E_0$ and the normalised carrier density $\tilde{n} = N/N_0 - 1$ and utilising Eqs. (2.5) and (2.6), the rate equations obtain the following form

$$\frac{\mathrm{d}A}{\mathrm{d}t} = \frac{1}{2}\{(1 - i\alpha)\frac{\gamma_c\gamma_n}{\gamma_s\widetilde{J}}\tilde{n} - (1 - i\beta)\gamma_p(|A|^2 - 1)\}A + F_A \tag{2.9}$$

$$\frac{\mathrm{d}\tilde{n}}{\mathrm{d}t} = \gamma_s\widetilde{J}(1 - |A|^2) - \gamma_s\tilde{n} - \gamma_n|A|^2\tilde{n} + \frac{\gamma_p\gamma_s\widetilde{J}}{\gamma_c}|A|^2(|A|^2 - 1) + F_{\tilde{n}}, \tag{2.10}$$

density, d is the active region thickness and e is the elementary charge. In Eq. (2.2) J is a more general pump rate used to describe both optically and electrically pumped lasers.

where $\widetilde{J} = (J - J_{th})/J_{th}$ is the pump rate normalised to the threshold value J_{th}. The differential and nonlinear gain relaxation rates γ_n and γ_p, respectively, are defined by

$$\gamma_n = \left(\frac{\partial g_r}{\partial N}\right) S_0 \tag{2.11}$$

and

$$\gamma_p = -\Gamma \left(\frac{\partial g_r}{\partial S}\right) S_0 \tag{2.12}$$

where $S_0 = \frac{2\epsilon_0 n^2 |E_0|^2}{\hbar\omega_0}$ is the steady-state photon density. The effect of nonlinear gain is to reduce the total gain. Therefore, the nonlinear gain relaxation rate γ_p in Eq. (2.12) is defined with a minus sign so that $\gamma_p > 0$. Also note that γ_n and γ_p are linear functions of the operating point. In this model, the above threshold operation of a class-B laser is determined by the following nine quantities: $\tilde{J}$, γ_s, γ_n, γ_c, γ_p, α, β, F_A, and $F_{\tilde{n}}$. Usually, in lasers, F_A dominates over $F_{\tilde{n}}$; therefore, $F_{\tilde{n}}$ is often omitted [36][**IV**]. Furthermore, β is expected to be small [37] although more recent experiments on semiconductor lasers indicate otherwise [38]. More often than not, β is ignored or $\beta = \alpha$ is used.

Equations (2.9) and (2.10) seem to define a three dimensional system. However, by expressing A in exponential form, i.e., writing $A = |A|e^{-i\phi}$, it can be seen that the phase ϕ decouples and what is left is a two-dimensional system for $|A|$ and $\tilde{n}$.

2.1.1 The Linewidth Enhancement Factor

The linewidth enhancement factor is defined as the ratio of partial derivatives, with respect to the carrier density, of the real and imaginary parts of the susceptibility[3]

$$\alpha = \frac{\partial\chi'/\partial N}{\partial\chi''/\partial N}. \tag{2.13}$$

Laser gain variations correspond to variations in $-\chi''$, and changes in the refractive index to changes in χ'. Therefore, α describes the coupling between gain and refractive index variations due to variations in the carrier density. Analogously, β describes the coupling between gain and refractive index variations due to variations in the intensity.

If a gas laser is forced to operate away from the gain peak, then a broadening of the linewidth is observed. Lax [40, 41] showed that this line broadening is due

[3] Often a minus sign is included in the definition. The sign depends on which time factor $e^{\pm i\omega t}$ is considered, since $\chi(\omega) = \chi(-\omega)^*$, i.e., $\chi'(\omega) = \chi'(-\omega)$ and $\chi''(\omega) = -\chi''(-\omega)$ [39]. In the introduced laser model the time factor $e^{-i\omega t}$ is considered, which means that gain corresponds to $-\chi'' > 0$.

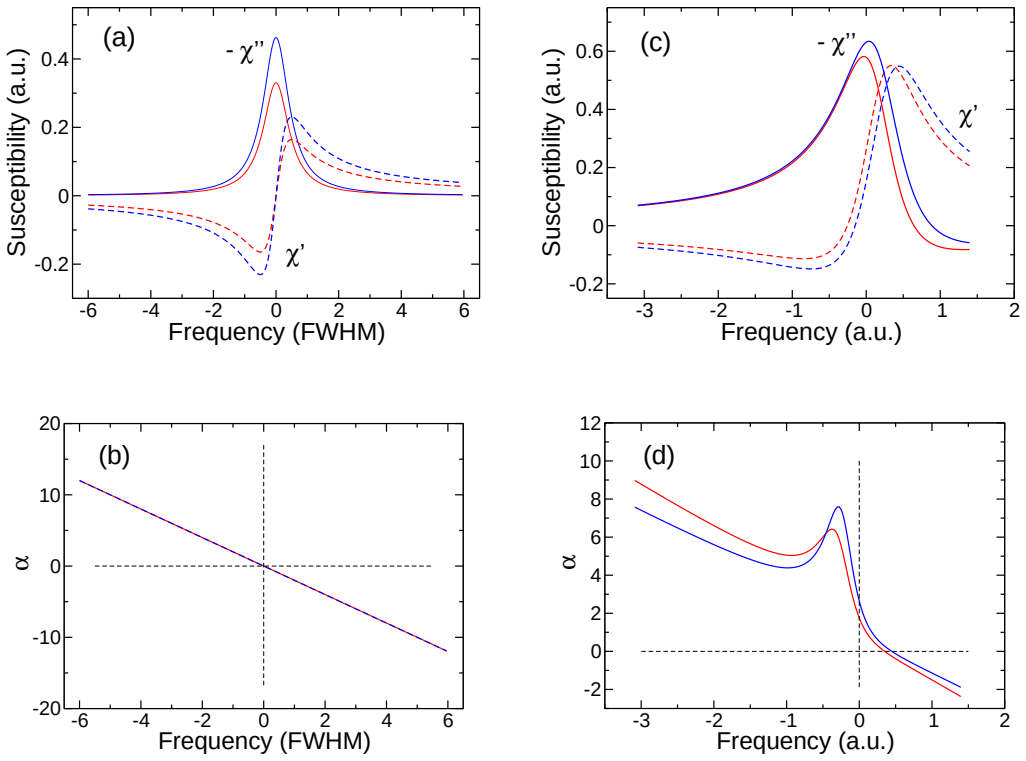

Fig. 2.1: Susceptibility and the linewidth enhancement factor as a function of frequency detuning from the gain peak for two different carrier densities drawn in blue and red with $N_{red} < N_{blue}$. For a symmetric Lorentzian gain profile α is zero at the gain peak (b). In semiconductor gain media the gain profile is asymmetric (c), which leads to $\alpha \neq 0$ at the gain peak. Note that (c) and (d) are only schematics of the type of behaviour that can be expected. The detailed behaviour is a complex function of the laser structure and materials used.

to the coupling of intensity and phase and results in a $(1+\alpha^2)$ enhancement of the linewidth. The situation is depicted in Fig. 2.1(a) for a symmetric Lorentzian gain profile. At the gain peak, the χ' curves go through zero and $\alpha = 0$ results. The real and imaginary parts of the complex susceptibility form a Hilbert transform pair (Kramers-Kronig relations) [42]. It is a general feature of this transformation that a symmetric gain profile leads to $\chi'(\omega = 0) = 0$. Away from the gain peak α is nonzero, as shown in Fig. 2.1(b). For a Lorentzian gain profile $\alpha = 2\Delta/\mathrm{FWHM} = \Delta/\Gamma_P$ where Δ is the cavity detuning from the gain peak, FWHM is the full width at half maximum of the gain profile, and Γ_P is the material polarisation decay rate, i.e., the inverse of the dephasing time. Therefore, α is related to the detuning parameter often found in gas and solid-state laser analysis. Traditional solid-state and gas lasers tend to be relatively long with small longitudinal mode spacings, which means that they operate very close to the gain peak unless forced to do otherwise. With approximately symmetric Lorentzian gain profiles $\alpha^2 << 1$ results.

In the early days of semiconductor lasers, there was an order of magnitude discrepancy between measured and theoretically predicted linewidths [43]. This discrepancy was resolved by Henry [44], who showed that α, which was thought to be small also for semiconductors, actually could take relatively large values, resulting in broadening factors $(1 + \alpha^2)$ as large as 10...40. In semiconductor gain media, the gain profile is asymmetric with $\alpha > 0$ also at the gain peak. This is illustrated in Figs. 2.1(c) and 2.1(d). Note that these graphs are only schematics of the type of asymmetry that can be expected. They were plotted using a bulk gain model presented in [45]. The exact gain profile is difficult to obtain from first principles owing to the semiconductor band structure and the complicated many-body carrier-carrier, carrier-hole and hole-hole interactions [46]. The susceptibility, and therefore also α, is a function of several quantities, including the carrier density, operating wavelength, temperature, gain material, and the geometry of the active region (bulk, quantum well, ...).

In the rate-equation model, α is introduced by assuming that the susceptibility varies linearly with carrier density, i.e., α is constant. The validity of this assumption has been investigated in [47] using more general Bloch equations. The authors of the cited paper come to the conclusion that a constant α can be used for free-running or modulated semiconductor lasers as long as the lasers are not biased too far below threshold. In other words, the carrier density must remain nearly constant. A more generalised model is needed whenever sub-picosecond pulses are present.

The linewidth enhancement factor is perhaps the most important semiconductor laser parameter. Besides the linewidth broadening already discussed, it also influences laser behaviour under optical injection and optical feedback. Furthermore, α is responsible for frequency chirping under high-speed current modulation

and for filamentation in broad-area high-power lasers [48]. Because of this, many techniques have been put forward over the years to measure α in semiconductors, some of which are presented in the upcoming chapters. Despite the abundance of techniques available, no systematic comparison between these techniques have been made – a shortcoming noted already in 1987 in an review paper by Osiński and Buus [49]. Since then, a number of new experimental schemes have been published, but still a comprehensive comparison between these techniques have been lacking. Article **I** of this Thesis presents the first extensive comparison between different techniques. In the article nine different methods are tested on a single VCSEL. Including the regeneratively amplified probe technique, which is discussed in Chapter 4, brings the total number of α-measurement techniques applied to the one and the same VCSEL up to ten.

By definition, α is a material parameter whose value depends on many factors, e.g., the carrier density, wavelength, temperature, etc. In article **I** all measurements are performed above or very close to threshold, and the mathematical formulae used to obtain expression for α have been derived from the laser rate equations. Therefore, in this context, α must be considered as a model parameter (device-α) somewhat 'detached' from its physical origin. There are, however, experimental techniques available that rely on the very definition of α, and these techniques measure what is called the material-α. Unfortunately, many of the more fundamental techniques, which are based on gain and refractive index measurements, cannot be applied to the VCSEL studied in this Thesis. Some of the techniques require the existence of many longitudinal modes inside the gain bandwidth and are, therefore, not applicable to VCSELs at all. Others require custom made devices, which means that commercial devices are unsuitable. In the exhaustive α-measurements planned within the COST action 288: "Nanoscale and ultrafast photonics" of the EU [50], different material-α and device-α techniques will be tested on many different laser structures. It will be interesting to see the results of those experiments, both in terms of the material-α vs device-α and in terms of the results in article **I**.

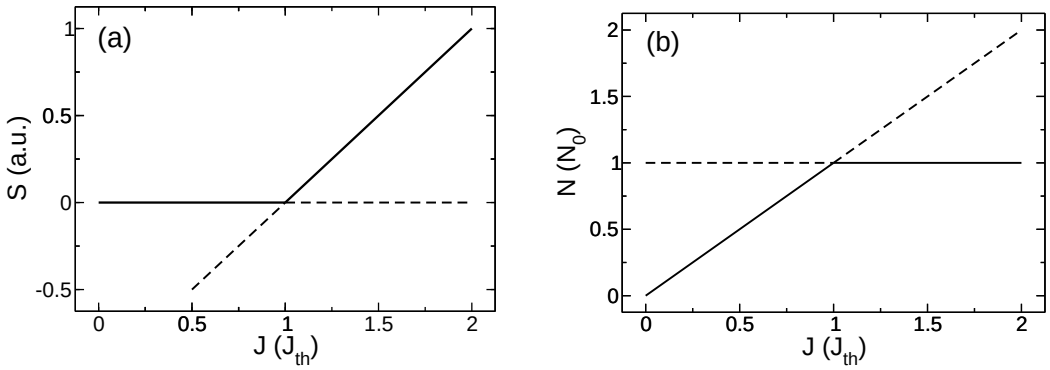

Fig. 2.2: Illustration of model solutions for S and N as a function of the pump rate. Here a linear recombination coefficient is used and spontaneous emission is ignored. Solid lines indicate stable solutions and dashed lines unstable solutions.

2.2 The Steady State

In order to get an overview of laser behaviour, some basic properties of the laser model are reviewed. To simplify the discussion, the noise terms and the nonlinear gain are neglected in this Section. Furthermore, a linear recombination rate is assumed. The steady states of the laser are easily found by putting the time derivatives of the rate equations to zero. This produces two branches of solutions:

$$\begin{aligned} S &= 0 \\ N &= \frac{J}{J_{th}} N_0 \\ \Delta\omega &= \alpha \frac{\Gamma}{2\gamma_s} \frac{\partial g}{\partial N} (J - J_{th}) \end{aligned} \tag{2.14}$$

and

$$\begin{aligned} S &= \frac{\Gamma}{\gamma_c} (J - J_{th}) \\ N &= N_0 \\ \Delta\omega &= 0. \end{aligned} \tag{2.15}$$

Here S is the photon density, $J_{th} = \gamma_s N_0$ and $\Delta\omega$ is a shift in the angular oscillation frequency. A stability analysis shows that solution (2.14) is stable when $J < J_{th}$ and (2.15) is stable when $J > J_{th}$. In Fig. 2.2 the stable and unstable solutions are represented with continuous and dashed lines, respectively. The two branches of solutions intersect at the lasing threshold in a transcritical bifurcation [51]. Above threshold $S > 0$ and below $S = 0$. In a real laser

spontaneous emission is always present, and because of that, the photon density is nonzero (but very small) also below the lasing threshold.

Below threshold, the LEF causes a blueshift of the laser frequency. This can be used to advantage when the value of this important parameter is sought for [**I**]. Equation (2.15) and Fig. 2.2(b) show that the carrier density is clamped above threshold to its value at threshold. This is a very important property of lasers, and it justifies the series expansions of the recombination rate and the gain made in Eqs. (2.5) and (2.6).

According to quantum mechanical many-body calculations, the peak gain in bulk semiconductor gain media is a linear function of the carrier density $g_{peak} = G_N(N - N_{tr})$ where N_{tr} is the carrier density at transparency [52]. Conventional EELs tend to operate close to the gain peak, since the cavity does not, in theory, discriminate between the relatively closely spaced longitudinal modes. In a DFB laser, and in a VCSEL in particular, the cavity determines the lasing wavelength. Therefore, these lasers can be forced to operate far from the gain peak where the gain is a nonlinear function of the carrier density. In quantum-well lasers even the peak gain is a nonlinear function of N. In this Thesis lasers are operated above or very near the threshold, where the carrier density is clamped, and without the presence of extremely short and high peak-power pulses. Therefore, the use of a linear gain model with respect to the carrier density is acceptable.

Nd:YVO_4 is an almost ideal four-level gain medium. If the lower level is completely ignored, then there will be gain as soon as there are electrons in the upper laser level, and this gain will increase linearly with the population inversion. Consequently, these lasers are often modelled with a gain $g = KN$ where K is a constant. The lower level does play a very important role when noise and modulation properties are considered. In [53] it is shown how the nonzero lower level lifetime gives rise to the nonlinear term in the expression for the gain. In short, another rate equation is written for the lower level population N_2. Due to the very short lifetime of this level, adiabatic elimination of N_2 can be done, which then results in gain suppression in proportion to the output intensity. In semiconductor lasers the origin of nonlinear gain is usually attributed to spectral hole burning and carrier heating [54]. The relative importance of the two different processes seems to depend on the laser type [55, 56]. Spectral hole burning is the formation of a dip in the gain profile around the lasing wavelength due to the reduction of carriers by stimulated emission. In carrier heating the electron and hole temperatures differ from the lattice temperature, which leads indirectly to gain suppression. Furthermore, in [57], it is shown how lateral carrier diffusion caused by spatial hole burning in semiconductor lasers also gives rise to nonlinear gain.

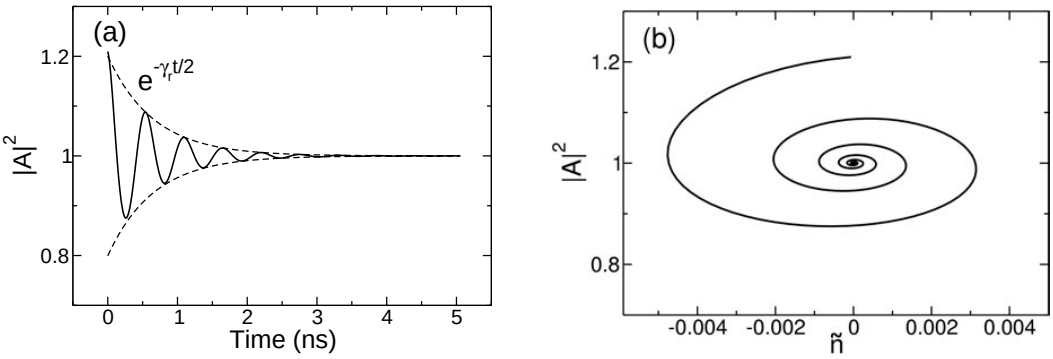

Fig. 2.3: After a perturbation the steady state is restored via relaxation oscillations. Oscillations of intensity as a function of time is shown in (a), and (b) shows the same oscillations in the $(\tilde{n}, |A|^2)$-plane.

2.3 Dynamics

If a semiconductor or a solid-state laser is perturbed from its steady state above threshold, then the steady state is restored via relaxation oscillations as illustrated in Fig. 2.3. Below threshold these lasers relax without oscillations [58]. The relaxation oscillation frequency $f_R = \Omega_R/2\pi$ is the characteristic frequency of lasers. A small signal analysis shows that

$$\Omega_R^2 = \gamma_c\gamma_n + \gamma_s\gamma_p \approx \gamma_c\gamma_n \approx \gamma_s\gamma_c\tilde{J} = \frac{1}{\tau_s}\frac{1}{\tau_c}\tilde{J} \tag{2.16}$$

where $\tau_s = \gamma_s^{-1}$ is the differential upper state lifetime and $\tau_c = \gamma_c^{-1}$ is the cavity lifetime. The first approximation follows from the fact that $\gamma_c \gg \gamma_p$. If the gain is simply written as $g = KN$, then $\gamma_n = \gamma_s\tilde{J}$ [59]. In semiconductors the first approximation is correct to within a few per cent, the latter, to within a few tens of per cent. In Nd:YVO_4 both approximations are accurate to a high degree. The damping of the relaxation oscillations is given by the relaxation rate

$$\gamma_r = \gamma_s + \gamma_n + \gamma_p. \tag{2.17}$$

The cavity lifetime τ_c of the VCSEL of articles **I** and **II** and of the EEL of article **V** is $\mathcal{O}(1$ ps), i.e., γ_c is $\mathcal{O}(10^{12}\text{s}^{-1})$. The upper level differential lifetime τ_s is $\mathcal{O}(1$ ns) and γ_s is $\mathcal{O}(10^9\text{s}^{-1})$. Hence the characteristic frequency f_R in semiconductor diode lasers is $\mathcal{O}(1$ GHz).

In the Nd:YVO_4 laser of articles **III** and **IV**, the cavity lifetime is $\mathcal{O}(100$ ps) and τ_s is 90 μs. These values yield relaxation oscillations of $\mathcal{O}(1$ MHz). The three orders of magnitude difference between the characteristic frequencies of these two types of lasers is mostly due to the five orders of magnitude difference in the

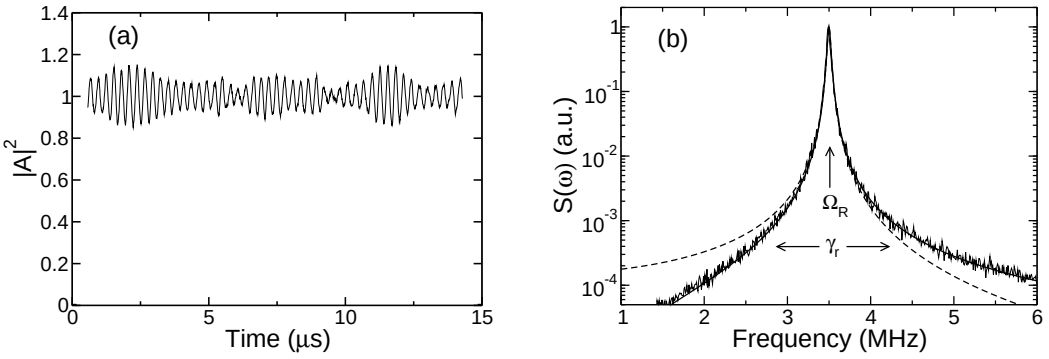

Fig. 2.4: Relaxation oscillations excited by noise in a free-running Nd:YVO_4 laser (a) and the corresponding power noise spectrum (b).

upper state lifetimes. Due to the long upper state lifetime of these solid-state lasers, they are often referred to as slow-inversion lasers.

In certain gas lasers, the relaxation oscillations can be overdamped, meaning that the lasers relax without oscillations. This happens approximately when $\tau_s \lesssim \tau_c$, i.e., when the cavity lifetime is longer than the upper level lifetime.

2.4 Noise

Noise due to spontaneous emission is the dominant noise source in semiconductor lasers [36]. The same applies for diode-pumped Nd:YVO_4 solid-state devices. Fourier transforming the linearised rate equations gives the following expression for the power noise spectral density

$$S(\omega) = \frac{(\frac{\gamma_c \gamma_n}{\gamma_s \tilde{J}})^2 D_{\tilde{n}}^2 + 4D_A^2(\omega^2 + (\gamma_s + \gamma_n)^2)}{(\Omega_R^2 - \omega^2)^2 + \omega^2 \gamma_r^2} \tag{2.18}$$

where $D_{\tilde{n}}^2 = \langle F_{\tilde{n}}(\omega) F_{\tilde{n}}^*(\omega) \rangle$ and $D_A^2 = \frac{1}{2}\langle F_A(\omega) F_A^*(\omega) \rangle = (4\pi |E_0|^2)^{-1} R_E$. A typical power time series is shown in Fig. 2.4(a) together with a power noise spectrum for an Nd:YVO_4 laser (b). The dashed line is calculated with $D_A^2 = 0$ and $D_{\tilde{n}}^2 > 0$, and the solid line with $D_A^2 > 0$ and $D_{\tilde{n}}^2 = 0$. The latter case gives an excellent fit to the experimental data and it can be concluded that the field noise due to spontaneous emission dominates. The location of the peak gives the relaxation oscillation frequency f_R and the width of the spectra gives the relaxation rate $\gamma_r = \gamma_s + \gamma_n + \gamma_p$. Power noise spectral measurements are thus an important technique for the characterisation of lasers. Since both γ_n and γ_p depend on the operating point of the laser, extrapolating γ_r to threshold gives the differential upper state decay rate γ_s (see, e.g., Fig. 2(b) in [**II**]). In article **IV** γ_r is measured using the above technique for the solid-state laser at $J = 3.5 J_{th}$

with the results that γ_p is an order of magnitude larger than γ_s and γ_n. This means that the nonlinear gain relaxation rate, which arises due to the short but nonzero lifetime of the lower laser level, actually dominates the damping rate.

The variance of the output power $\langle \Delta p^2 \rangle$ can be related to the noise spectral density

$$\langle \Delta p^2 \rangle = \frac{1}{2\pi} \int_{-\infty}^{\infty} S(\omega) d\omega \simeq \frac{2D_A^2}{\gamma_r}, \tag{2.19}$$

which is proportional to D_A^2 when $D_{\tilde{n}}^2$ is ignored. Thus a measurement of the noise spectral density and power variance yields D_A^2. The power variance of Nd:YVO_4 lasers is easy to measure because of the low frequencies involved. In article **IV** a value of $D_A^2 = 750\text{s}^{-1}$ was obtained.

The carrier noise $F_{\tilde{n}}$ has a negligible influence on laser linewidths. Based on what was described above, its influence on the power variance is also at least an order of magnitude smaller than that of the field noise F_A. However, according to numerical studies in [60], carrier noise may play an important role in the dynamics of coupled lasers. In the cited paper a semiconductor laser with delayed optical feedback was studied, and it was found that, under certain operating conditions, the carrier noise determined the stable dynamical states of the system. The authors conjectured that carrier noise might also be important for lasers with optical injection. In Chapters 4 and 5 and in more detail in article **IV** and [61], experiments on optically injected Nd:YVO_4 lasers are compared to predictions of the rate-equation model introduced above. In the simulations carrier noise is excluded, and yet no discrepancies between simulations and experiments is found. Hence, at least for these types of experiments and lasers, carrier noise is of minor importance.

2.4.1 Frequency Linewidth

A fundamental property of any laser is the frequency linewidth of the emitted light. According to the Wiener-Khintchine theorem, the optical spectrum can be obtained as the Fourier transform of the autocorrelation function

$$G_E(\tau) = \frac{\langle E(t+\tau)E^*(t) \rangle}{\langle E(t)^2 \rangle}. \tag{2.20}$$

The calculation of the optical spectrum via the autocorrelation function from the laser rate equations has been presented in [62]. The result is that above threshold the spectrum consists of a narrow central peak and weak sidebands due to the relaxation oscillations. For linewidths $\Delta\nu \ll \gamma_r$ the line profile is Lorentzian with a FWHM linewidth

$$\Delta\nu = \frac{D_A^2}{2\pi}(\alpha^2 + 1). \tag{2.21}$$

Equation (2.21) is commonly referred to as the modified Schawlow-Townes formula. For the above Nd:YVO_4 laser, Eq. (2.21) predicts a frequency linewidth of only 120 Hz ($\alpha^2 \ll 1$). In practise, however, the linewidth is limited to the 10-100 kHz level by mechanical vibrations and, especially, refractive index variations due to temperature fluctuations [63].

In order to see which properties of lasers affect their linewidths, the Langevin noise spectral density D_A^2 must be expressed in terms of other laser parameters. Let R_{sp} denote the rate of spontaneously emitted photons into the lasing mode. By expressing Eq. (2.9) in terms of the number of photons in the lasing mode $P_\#$, it can be shown that [36]

$$R_{sp} = 2D_A^2 P_\#. \tag{2.22}$$

Experimentally, $P_\#$ can be obtained from the relation

$$\gamma_m P_\# = \frac{P_{out}}{\hbar\omega} \tag{2.23}$$

where P_{out} is the total output power and γ_m is the cavity loss rate due to the mirrors

$$\gamma_m = -\frac{\ln(R_1 R_2)}{t_{RT}} \tag{2.24}$$

where R_1 and R_2 are the mirror reflectivities and t_{RT} is the round-trip time in the cavity.[4] According to quantum theory, the rate of photons emitted by stimulated emission R_{st} equals the number of photons in the mode multiplied by the rate of spontaneously emitted photons into the mode, i.e., $R_{st} = P_\# R_{sp}$. In a steady state above threshold the rate of stimulated emission must equal the number of photons lost per unit time, which is given by $\gamma_c P_\#$. From this it follows that $R_{st} = \gamma_c P_\#$ and $R_{sp} = \gamma_c$. If the inversion is not complete, then there will be absorption, which reduces the net rate of stimulated emission. This is taken into account by introducing the inversion factor $n_{sp} \geq 1$ so that

$$R_{sp} = n_{sp}\gamma_c \tag{2.25}$$

above threshold. In other words, the reduction of net stimulated emission caused by absorption enhances the relative amount of spontaneous emission. From Eqs. (2.22), (2.24) and (2.25) the inversion factor for the Nd:YVO_4 laser can be computed. The result is $n_{sp} \approx 1.0$ as it should for a nearly ideal four-level laser. In semiconductors $n_{sp} = 1.5...2.5$. In article **II** a value of $n_{sp} = 1.9$ is deduced for the VCSEL. The spontaneous emission rate can also be enhanced by other factors,

[4] The cavity decay rate γ_c includes all losses whereas γ_m is the loss rate due to the output coupling only.

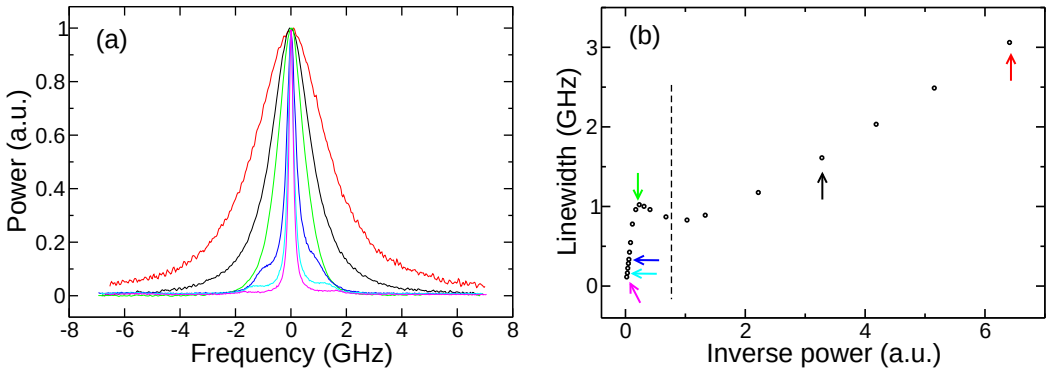

Fig. 2.5: (a) Laser line profile as recorded with a Fabry-Pérot interferometer. For the narrowest linewidths plotted, the finite finesse (≈ 200) must be taken into account when estimating the real laser linewidth. (b) Linewidth (FWHM) as a function of inverse output power. The dashed line marks the threshold.

including unevenly distributed losses in the cavity, which lead to nonorthogonal eigenmodes [64], as well as phase-front curvature in gain guided lasers [65].

Using the above formulae, the frequency linewidth can be expressed as

$$\Delta\nu \approx \frac{n_{sp}\gamma_c\gamma_m\hbar\omega_0}{4\pi P_{out}}(1+\alpha^2). \tag{2.26}$$

The cavity lifetimes of the VCSEL of articles **I** and **II** and of the EEL of article **V** were measured to be around 3 ps, i.e., a factor of 20 smaller than the cavity lifetime of the Nd:YVO_4 laser [**IV**]. When the LEF is around five (α^2+1) is near 30. As a consequence, for similar output powers linewidths of the order of 1 MHz can be expected in semiconductor lasers. The four orders of magnitude difference between the linewidths of the semiconductor lasers and the solid-state laser used in this work is, therefore, accounted for by the differences in the LEF and the different cavity lifetimes.

Far below threshold, the linewidth is given by the Schawlow-Townes formula [66]

$$\Delta\nu = \frac{D_A^2}{\pi} = \frac{R_{sp}}{2\pi P_{\#}}, \tag{2.27}$$

and what the transition to the modified Schawlow-Townes formula, Eq. (2.21), looks like depends on the LEF [67]. For $\alpha \gtrsim 3$ the transition is nonmonotonous. Such a behaviour has been observed in DFB lasers in [66, 68, 69] and in a VCSEL for the first time in article **II**. Figure 2.5 shows the measured linewidth versus inverse power across the threshold transition. According to Eqs. (2.21) and

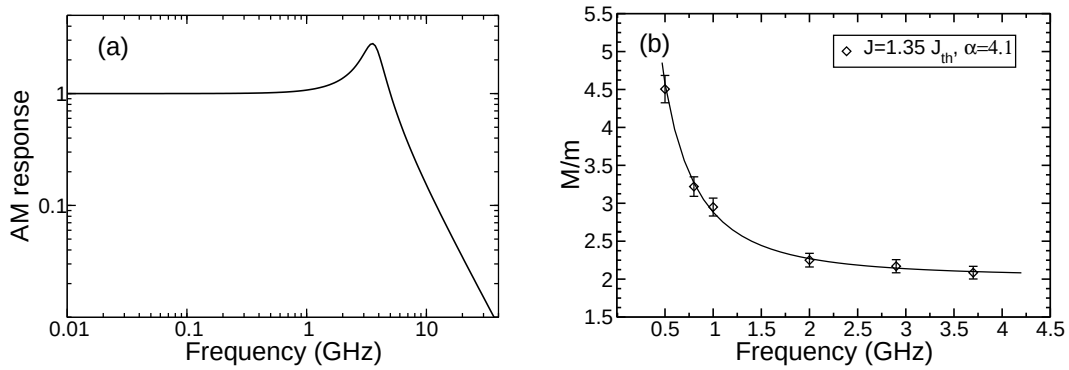

Fig. 2.6: (a) Intrinsic AM response of a VCSEL calculated from Eq. (2.28) using parameters for a 760-nm VCSEL [**II**]. (b) Measured FM/AM response together with fits to Eq. (2.30) for the same laser [**I**].

(2.27), the ratio of the slopes above and below threshold is

$$\frac{\alpha^2+1}{2}.$$

With this relation, α can be estimated from linewidth versus inverse power data [70]. Figure 2.5(b) yields $\alpha = 5.0 \pm 0.4$.

2.5 Pump Modulation

When a small sinusoidal modulation $\Delta J = \frac{1}{2}J_1 e^{-i\Omega_M t}$ + c.c. with angular frequency $\Omega_M = 2\pi f_M$ is superimposed on the pump J, lasers respond by modulating the power Δp and the phase of the electromagnetic field. Let $\Delta p = \frac{1}{2}p_1 e^{-i\Omega_M t}$ + c.c. and $\tilde{n} = \frac{1}{2}\tilde{n}_1 e^{-i\Omega_M t}$ + c.c. where p_1 and $\tilde{n}_1$ represent small perturbations to the steady-state values. A small-signal analysis yields

$$p_1 = \frac{\frac{\gamma_c \gamma_n J_1}{J_{th}\widetilde{J}}}{(\Omega_R^2 - \Omega_M^2) - i\Omega_M \gamma_r}. \tag{2.28}$$

The amplitude modulation[5] (AM) response equals $|p_1|$ and is illustrated in Fig. 2.6(a). Since normalised units are used, i.e., average power is 1, this quantity also equals the AM index m.[6] Beyond the relaxation oscillation frequency the response of the laser drops fast, which, e.g., limits the attainable bitrates in

[5] Here amplitude refers to the amplitude of the sinusoidal power modulation and not to the amplitude of the electric field.

[6] The AM index is defined as the amplitude of the power modulation normalised to the average power.

high speed telecommunication systems. In neodymium doped solid-state lasers the long lifetime of the upper state limits the modulation frequencies to a few MHz, making such lasers unsuitable for optical communication systems based on directly modulated lasers.

The AM response formula, Eq. (2.28), can usually not be used to experimentally extract laser parameters, since the microwave response of the laser mount and casing is often unknown. The parasitics can be avoided with special arrangements, though. In [71, 72], the carrier density is modulated by external light shone directly onto the active region. To avoid optical injection and cavity effects, the modulating light must be directed perpendicularly to the cavity and tuned far away from the frequency of the lasing mode. In the cited papers light from a krypton laser at 753 nm was mixed with light from a dye laser to produce beat frequencies in the GHz regime. The experimental data for the studied 840-nm edge-emitter were in excellent agreement with the small signal AM response function deduced from the rate equations.

2.5.1 Frequency Modulation

Let $A = |A|e^{-i\phi}$ where $\phi = \frac{1}{2}\phi_1 e^{-i\Omega_M t} + \text{c.c.}$ is the phase of the electric field. Then ϕ_1 is given by

$$\phi_1 = \frac{1}{2}[\alpha + \frac{i\gamma_p}{\Omega_M}(\alpha - \beta)]p_1, \tag{2.29}$$

and the angular frequency chirp is $\Delta\omega = |\phi_1|\Omega_M$. Frequency modulation (FM) is often characterised by the FM index M, which is defined by $M = \Delta\omega/\Omega_M$. A useful formula is obtained from the ratio of the FM and AM indexes

$$\frac{M}{m} = \frac{\alpha}{2}\sqrt{1 + \left(\frac{\alpha - \beta}{\alpha}\right)^2 \left(\frac{\gamma_p}{\Omega_M}\right)^2}, \tag{2.30}$$

which is fitted to experimental data from the VCSEL in Fig. 2.6(b) [**I**]. As the modulation frequency increases, the FM to AM ratio approaches $\alpha/2$. This feature has been used extensively in the literature to determine α in semiconductor lasers, and many different techniques have been put forward over the years to measure the FM/AM ratio, starting with the seminal paper by Harder *et al.* [73] and the introduction of the nonlinear gain contribution (with $\beta = 0$) in [74]. Equation (2.30) represents also a straightforward method to measure γ_p provided that the nonlinear index contribution can be ignored, i.e., $\beta = 0$. In articles **I** and **V** the FM/AM technique is utilised to measure α in the VCSEL and in the EEL, respectively, and in article **III** the method is extended to the Nd:YVO_4 solid-state laser case.

Equation (2.30) is only valid at high frequencies. At low frequencies the chirp is dominated by the temperature dependence of the refractive index and cavity

length. Article **III** shows one simple way the temperature dependence can be introduced into the model via the cavity angular resonance frequency ω_c. Let ΔT be a small change in temperature caused by pump modulation. The evolution of ΔT is governed by the heat conduction equation

$$\rho c_p \frac{\partial \Delta T}{\partial t} = \kappa_T \nabla^2 \Delta T + \Delta Q \tag{2.31}$$

where κ_T is the thermal conductivity, c_p is the heat capacity, ρ is the density, and ΔQ is a small change in the amount of heat generated in a unit volume per unit time. Equation (2.31) can be integrated over the lasing mode to produce an equation for an effective temperature ΔT_e. Temperature decay (or equalisation) is performed by the Laplacian, which is here approximated simply by a decay rate γ_T. This gives

$$\frac{\partial \Delta T_e}{\partial t} = -\gamma_T \Delta T_e + \Delta Q_e. \tag{2.32}$$

Finally, if a linear dependence between temperature and cavity resonance frequency is assumed, i.e., $\Delta\omega_c = \kappa_{\omega T} \Delta T_e$, and a sinusoidal modulation is applied, i.e, $\Delta Q_e = \frac{1}{2} Q_{e0} \exp(-i\Omega_M t) + c.c.$, then

$$\Delta\omega_{c0} = \frac{\kappa_{\omega_T} Q_{e0}}{-i\Omega_M + \gamma_T}. \tag{2.33}$$

The frequency response thus equals the response of a passive first-order RC low-pass filter of electronics with a -3 dB cutoff frequency of $f_M^{-3dB} = \gamma_T / 2\pi$. An order of magnitude estimate for the cutoff frequency follows from the heat conduction equation. The Laplacian can be approximated by $L_x^{-2} + L_y^{-2} + L_z^{-2}$ where L_i, $i = x, y, z$, are the characteristic length scales in the directions of the corresponding coordinate axes. In lasers the lateral dimensions (mode width) are usually much smaller than the longitudinal dimension (cavity length), the exception being VCSELs where the cavity length and mode waist are of the same magnitude. Nevertheless, an order of magnitude estimate for the Laplacian is $2w^{-2}$ where w is the mode width (waist). Then

$$\gamma_T \approx \frac{2\kappa_T}{w^2 c_p \rho} \tag{2.34}$$

is obtained. In the Nd:YVO_4 laser w is of the order of 100 μm, giving f_M^{-3dB} $\mathcal{O}$(100 Hz). The cutoff frequency is very low; however, the temperature induced FM is so strong and the population inversion induced FM so small that the temperature variation dominates the frequency response up to 1 MHz [**III**]. For VCSELs the characteristic length scale is a few μm, giving cutoff frequencies of the order of 100 kHz. Preliminary measurements on a 760-nm VCSEL in the

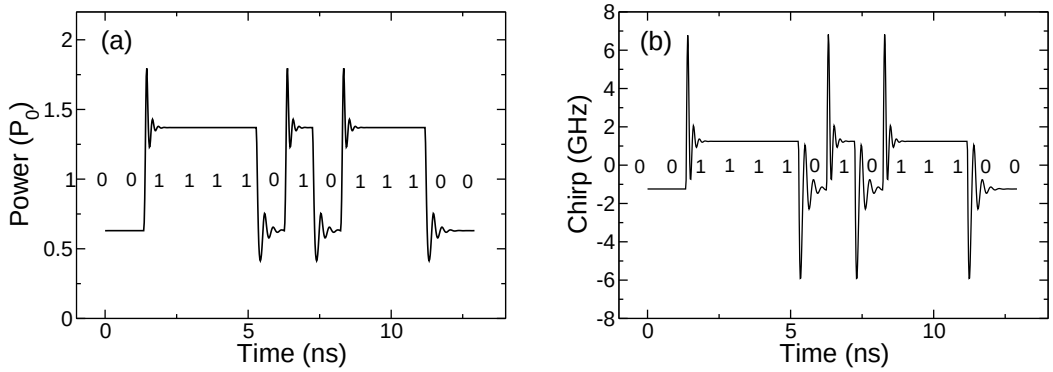

Fig. 2.7: A noiseless VCSEL ($f_R = 4.4$ GHz, $\alpha = 4$) modulated with an ideal 1 Gbit/s NRZ pseudo-random sequence: (a) amplitude modulation and (b) frequency chirping.

frequency range 100 kHz - 4 GHz gave a cutoff frequency of roughly 200 kHz. The overall agreement between the model and the data was good despite the rough approximations made above. In semiconductors the temperature response dominates the FM below 10-100 MHz (depending on laser structure). In the literature more detailed models of temperature response have been developed, which also take into account specific cavity structures, mode profiles and so on.

2.5.2 Large-Signal Modulation

Figure 2.7(a) illustrates relaxation oscillations that occur when a semiconductor laser is modulated with an ideal 1 Gbit/s non-return-to-zero (NRZ) pseudo-random sequence (noise and temperature neglected). As the modulation frequency is increased, the 'ringing' of the output intensity starts to interfere with the next symbol to be transmitted. This leads to inter-symbol interference (ISI). The ringing can be reduced by reshaping the drive current so that the output intensity behaves as smoothly as possible (see, e.g., [75] and references therein). With $\alpha > 0$ amplitude modulation is accompanied by frequency modulation, as shown in Fig. 2.7(b). The frequency chirping is detrimental to optical fibre communication systems, since group velocity dispersion (GVD) in fibres causes chirped pulses to broaden in time as they propagate. Hence, reducing the value of α in semiconductor lasers is of some technological importance. Furthermore, if α could be pushed down to zero, then an order of magnitude reduction in the linewidths of free-running semiconductor lasers would result.

On the other hand, if $\alpha \gg 1$, then pump-modulation results in close to pure frequency modulation. In [76] an effective LEF of almost 60 was measured at a certain bias current in a quantum-dot laser. Such a large value was measured

just below the operating point at which the ground state population of the dots became filled. This filling effect reduced the differential gain, which in turn reduced AM and increased the FM/AM ratio dramatically. As a consequence, the authors of the cited paper were able to produce frequency-shift keyed (FSK) communication signals in a directly modulated semiconductor laser. For more details on pump-modulation dynamics with relation to the LEF in quantum-dot lasers, the reader is referred to [77].

The above discussion on pump-modulation response brings part (i) of this Thesis to end. The upcoming third chapter gives a brief historical introduction to part (ii), where the dynamics of coupled lasers, unidirectionally coupled lasers in particular, is at the centre of attention.

3. COUPLED OSCILLATORS

In 1660, C. Huygens together with The Royal Society began working on the major technological challenge of that time, the longitude problem; that is, they wanted to find an accurate way of determining longitude for navigation at sea [78]. Huygens had invented the pendulum clock in 1657, and he was convinced that, with proper design, these clocks could be made accurate and robust enough for sea travel, thereby solving the longitude problem.[1] The continuous operation of an on board clock was vital to the determination of longitude. In case the clock stopped or required maintenance, another clock would be needed to keep accurate timing. The practical requirement of redundancy led Huygens to study two clocks operating at the same time. In a letter to The Royal Society in 1665, Huygens reported on "an odd kind of sympathy perceived by him in these watches suspended by the side of each other". Huygens found that two pendulum clocks with a common frame synchronised spontaneously. After disturbing one of the clocks, the synchronised state was re-established half an hour later, and the two clocks remained synchronised indefinitely. After a series on new experiments, Huygens was able to show that small vibrations in the common frame supporting the two oscillators was the cause for the phase locking.

The coupling between the two pendulum clocks was bidirectional. A more simple coupled system is that of unidirectional coupling. A nice example of this is the coupling between the circadian rhythms of biological organisms and the rotation of planet Earth [79]. Most, if not all, biological systems have internal clocks that regulate their lives. For example, the leaves of a haricot bean plant move up and down in concert with the time of day. The motion is regulated by the plant's circadian clock, but it is locked to the time of day via the environmental coupling. If the plant is moved into a room with constant environmental conditions, i.e., if the coupling to the Earths rotation is removed, then the motion will continue but the phase of the oscillation will drift with respect to the time of day.

[1] Location at sea is determined by longitude and latitude. Latitude can be determined by measuring the elevation of stars, e.g., Polaris, the North star, in the northern hemisphere. For Polaris, the elevation equals the geographic latitude. Determination of longitude is more problematic. Local time can always be found by, e.g., observing the sun, but to accurately determine longitude, the time at a reference location is also needed. For this purpose sailors needed accurate clocks to follow the time at a reference point.

Injecting a weak signal into an oscillator can produce, besides locking, a wealth of other interesting and useful phenomena in all kinds of self-sustained oscillators, including lasers. Locking between lasers was achieved for the first time already in 1966 [80]. In that experiment two single-mode He-Ne lasers (class A) operated in a master-slave configuration, where light from the master is injected unidirectionally into the cavity of the slave laser. The results of the experiment were in qualitative agreement with a general theoretical result by R. Adler in 1946, which relates the locking bandwidth $\Delta\omega_{lb}$ of a self-sustained oscillator to the injected signal amplitude E_i

$$\Delta\omega_{lb} = \frac{\omega_0}{Q}\frac{|E_i|}{|E_0|} \tag{3.1}$$

where E_0 and ω_0 are the free-running amplitude and angular oscillation frequency, respectively, and Q is the quality factor [81]. Equation (3.1) is derived with the restriction that only the phase of the oscillation is allowed to vary. In reality, the amplitude will also vary; however, under low level injection, the amplitude stays nearly constant due to the gain saturation effect present in self-sustained oscillators.

Far away from the locking region, the phasor of the slave laser, compared to the master, will rotate with a constant speed that corresponds to the frequency detuning. When the locking boundary is approached, the phasor, as it rotates, begins to spend more and more time at a certain angle while traversing other parts of the complex plane quickly. When the locking boundary is reached, the phasor makes a complete stop. This means that the phase difference between the master and the slave becomes a constant, i.e., that the slave is phase locked to the master. In time space the slave laser's behaviour en route to locking is nonlinear, with long smooth sequences periodically interrupted by more erratic behaviour. In frequency space the slave laser's oscillation frequency appears to be pulled towards the master's frequency. Examples of these will be given in Chapters 4 and 5, where the dynamics of coupled lasers is discussed.

Mathematically, the transition to locking in Adler's model happens via a saddle-node bifurcation. When the amplitude of the slave oscillator is also allowed to vary, locking can also take place via a Hopf bifurcation. These, and other types of bifurcations, are discussed in Chapter 4.

3.1 Coupled Class-B Lasers

A free-running single-mode class-B laser does not exhibit any complex behaviour.[2] If the laser is perturbed from its steady-state, then the steady state is restored via

[2] The Poincaré-Bendixson Theorem of mathematics states that only fixed-point or periodic solutions exist for an autonomous first-order differential equation in two dimensions [82].

relaxation oscillations. However, if a third degree of freedom can be introduced, a class-B laser can be driven into complicated dynamical states. The dimensionality can be raised to three in a number of ways, e.g., by injecting an external optical field or by making one of the parameters time dependant, i.e., by making the two dimensional system nonautonomous. An injected field prevents the phase of the EM field from decoupling, which then provides the necessary third degree of freedom.[3] The time dependence of a parameter can be removed by defining a third variable, say $z(t)$, with the equations $\dot{z} = 1$ and $z(0) = 0$, so that the time t is replaced by the new variable $z = t$. The new system is then autonomous and three dimensional [83]. Chaos in an optical device was first predicted in 1980 by Ikeda *et al.* [84], who investigated numerically the transmission properties of a ring cavity with a nonlinear dielectric element. However, chaotic dynamics was first experimentally observed in a loss modulated CO_2 laser (class B) by Arecchi *et al.* in 1982 [85].

The dimensionality can be raised also by other means, e.g., by opto-electronic and optical feedback (Fig. 3.1). In opto-electronic feedback, the output power is converted to a current and fed back to the laser. Both positive and negative opto-electronic feedback have been studied [86]. In optical feedback part of the output from the laser is fed back into the cavity of the laser. In these cases the system of equations becomes infinite dimensional, since a unique solution requires, in principle, the initial condition to be specified on a continuous time interval (corresponding to the delay of the feedback process). Optical feedback in single-mode semiconductor lasers is usually analysed in terms of the Lang-Kobayashi equations [87].

A phenomenological classification of different optical feedback regimes has been presented in [88]. At very low feedback levels, regime I, no instabilities exist. Depending on the feedback phase, broadening or narrowing of the linewidth is observed as are shifts in the oscillation frequency and output power. This regime can be used to advantage in interferometry [89]. For example, movement of a distant reflector can be monitored by reflecting a small part of the light back into the laser cavity. Any movement of the reflector will cause a phase shift in the feedback light and this will alter the frequency and output power of the laser.

With increasing feedback levels, regime II, mode-hopping between different longitudinal external cavity modes is seen as a function of the feedback phase. The mode hopping property can be utilised in the characterisation of lasers, e.g., to measure the LEF in a semiconductor laser [90][**I**]. In regime III large linewidth reductions and stable operation is obtained irrespective of the feedback phase. This regime has important applications in extended cavity diode lasers, where

[3] In other words, the injected field provides a time reference, a clock, which breaks the time invariance of the equations and turns the phase, with respect to the injected field, into an important variable.

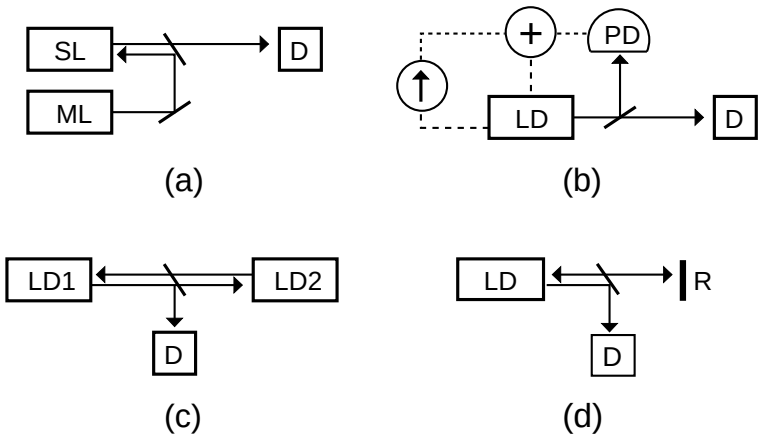

Fig. 3.1: Schematics of a few setups often used in the study of laser dynamics. Solid and dashed lines indicate optical and electrical paths, respectively. (a) unidirectionally coupled lasers (optical injection); (b) positive opto-electronic feedback; (c) mutually coupled lasers; and (d) optical feedback. Symbols as follows; LD: laser diode; ML: master laser; SL: slave laser; PD: photodiode; D: measurement apparatus (of appropriate type); R: reflector.

feedback is used to reduce the natural linewidth of semiconductor lasers by several orders of magnitude. In the experiments related to article **V**, a grating feedback semiconductor laser operating in this regime was used as the master laser.

In regime IV strong instabilities exist with multiple external cavity modes and linewidths of the order of 10 GHz. This regime has attracted much attention in recent years due to the presence of interesting complex dynamics. The chaotic output can be put to use in chaos communication experiments, where messages are 'hidden' in chaotic carriers. Finally, if the faced reflectivity R is much smaller than that of the external mirror R_{ext}, i.e., the feedback is very strong (regime V), then the laser cavity is essentially formed by the external cavity, R acting only as a perturbation.

In this Thesis the focus is on optical injection, i.e., unidirectional coupling. Optical feedback from a reflector (in regime II) as well as filtered optical feedback have only been applied in laser characterisation, more specifically, to measure the LEF in article **I**. In the next chapter the rate-equation model introduced in Chapter 2 is complemented with an injected optical field. It is shown how low level optical injection can also be used for parameter extraction. When the injection strength is increased, a tremendous variety of interesting and potentially useful dynamics is revealed.

4. OPTICALLY INJECTED LASERS

An injected optical field can be introduced into the model of Chapter 2 by adding a term $\eta E_i e^{-i\Omega t}$ to the right hand side (R.H.S.) of Equation (2.1) [91]. Equation (2.9) for the normalised field amplitude then becomes

$$\frac{\mathrm{d}A}{\mathrm{d}t} = \frac{1}{2}\{(1-i\alpha)\frac{\gamma_c\gamma_n}{\gamma_s\widetilde{J}}\tilde{n} - (1-i\beta)\gamma_p(|A|^2-1)\}A + \kappa e^{-i\Omega t} \tag{4.1}$$

where $\kappa = \eta|E_i|/|E_0|$ is the injection rate and $\Omega = 2\pi(\nu_{ML} - \nu_{SL})$ is the angular frequency detuning between the master and the slave laser. The time dependent injection term makes the model nonautonomous; however, it can be transformed back into an autonomous form by rewriting it in terms of $a = Ae^{i\Omega t}$ to yield

$$\begin{aligned}\frac{\mathrm{d}a}{\mathrm{d}t} &= [\frac{1}{2}\{(1-i\alpha)\frac{\gamma_c\gamma_n}{\gamma_s\widetilde{J}}\tilde{n} - (1-i\beta)\gamma_p(|a|^2-1)\} + i\Omega]a \\ &\quad +\kappa \qquad (4.2)\\ \frac{\mathrm{d}\tilde{n}}{\mathrm{d}t} &= \gamma_s\widetilde{J}(1-|a|^2) - \gamma_s\tilde{n} - \gamma_n|a|^2\tilde{n} + \frac{\gamma_p\gamma_s\widetilde{J}}{\gamma_c}|a|^2(|a|^2-1). \qquad (4.3)\end{aligned}$$

Equations (4.2) and (4.3) form a three dimensional nonlinear system that exhibits complicated nonlinear dynamics. In Chapter 2 the reference frequency was the free-running frequency of the laser. The above transformation means that the reference frequency is changed to the oscillation frequency of the master laser, i.e., a fixed-point solution with $\mathrm{d}a/\mathrm{d}t = \mathrm{d}\tilde{n}/\mathrm{d}t = 0$ now means that the slave laser is locked to the master.

Similarly, a model for a laser with optical feedback is obtained simply by adding a term $\eta E(t-\tau)$ to the R.H.S. of Eq. (2.1). Here τ is the round trip time and η describes the coupling of the feedback light into the laser mode.

The rate equations of an injected class-B laser exhibit very complicated solutions, and approximations are usually needed in order to analytically gain insight into laser behaviour. At very low injection rates where the external field can be treated as a perturbation, analytical formulae can be found that successfully describe the nonlinear interactions taking place within the laser cavity. At higher injection rates the equations must be analysed numerically, although exceptions do exist. This chapter presents analytical results valid for low power injection

together with numerical techniques that can be utilised at higher powers where the external field can no longer be treated as a perturbation.

4.1 Small-Signal Regime

According to Eq. (3.1), oscillators will lock to injected signals no matter how weak the coupling is made, but the locking range shrinks in proportion to the injection rate, i.e., in proportion to the square root of the injected power. This section presents laser behaviour under weak injection both inside and outside the locking range.

4.1.1 Regenerative Amplification and Four-Wave Mixing

Low power optical injection can be used to advantage in laser characterisation. Far from the locking region, very low power injection causes only a perturbation of the laser. Solutions of the form

$$A(t) = 1 + A_r e^{-i\Omega t} + A_f e^{i\Omega t} \quad (4.4)$$

$$\tilde{n}(t) = \tilde{n}_1 e^{-i\Omega t} + \tilde{n}_1^* e^{i\Omega t} \quad (4.5)$$

to Eqs. (4.1) and (2.10) can then be sought for [92]. Here A_r, A_f and $\tilde{n}_1$ represent small perturbations to the free-running field and carrier density, respectively.[1] This ansatz yields a useful expression for the regeneratively amplified field A_r [92, 93]

$$|\frac{A_r}{A_i}|^2 = |\frac{\eta}{\Omega}|^2 \frac{[-\Omega^2 + \frac{\Omega_R^2}{2} + \beta\Omega\gamma_p]^2 + [\Omega\gamma_r - \frac{\Omega\gamma_p}{2} - \frac{\alpha\Omega_r^2}{2} - \frac{(\beta-\alpha)(\gamma_r-\gamma_p)\gamma_p}{2}]^2}{(-\Omega^2 + \Omega_R^2)^2 + \Omega^2\gamma_r^2}. \quad (4.6)$$

The above equation is depicted in Fig. 4.1 together with experimental data for the VCSEL [**I**, **II**]. The equation is sensitive to Ω_R and γ_r, but the other parameters cannot be obtained directly. If γ_p is fixed to a known value, then the equation yields estimates for α as well. For the VCSEL this procedure gave $\alpha = 5.1 \pm 0.5$, in agreement with values obtained with various other methods in article **I**.

Above, the regeneratively amplified field was considered. A somewhat similar expression is obtained for the four-wave mixing field A_f, which is produced by the injection induced carrier pulsation. However, the A_f component is symmetric and its shape is independent of α, which makes it less interesting than the A_r component.

[1] Here it is more convenient to keep the reference frequency at the slave laser's free-running frequency. Hence Eqs. (4.1) and (2.10) are used instead of (4.2) and (4.3).

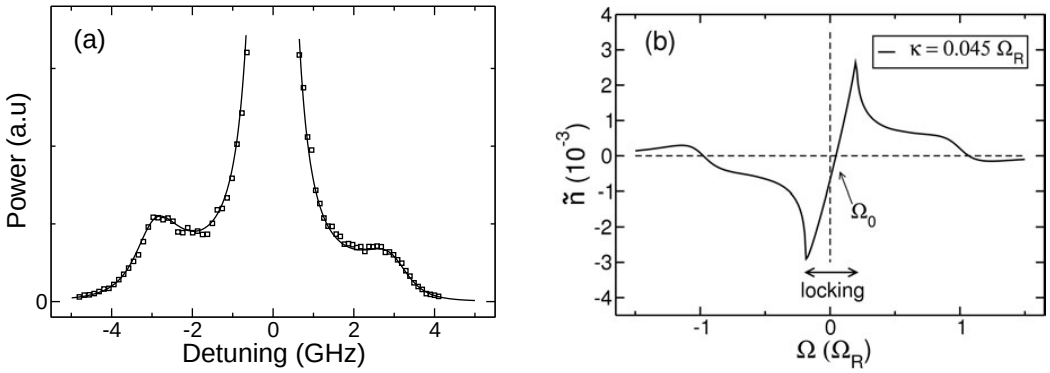

Fig. 4.1: (a) Regenerative amplification of a weak probe as a function of detuning for the VCSEL together with a fit to Eq. 4.6. (b) Schematic of carrier density variation across the locking range under weak injection.

4.1.2 Locking

The locking region at low injected powers can be found by putting the time derivatives of the linearised equations to zero. This gives

$$\Delta\omega_{lb} = 2\kappa\sqrt{1+\alpha^2} = \frac{\omega_c}{Q}\frac{|E_i|}{|E_0|}\sqrt{1+\alpha^2} \tag{4.7}$$

where $Q = \omega_c/\gamma_c$ is the quality factor of the empty cavity.[2] Comparing this to Eq. (3.1), it can be seen that the above formula contains an additional factor of $\sqrt{1+\alpha^2}$. In Eq. (3.1) it was assumed that the injected field does not alter the resonance frequency of the oscillator. But when $\alpha > 0$ a change in the carrier density due to the injected field will shift the cavity resonance frequency, which in turn gives an additional contribution to the locking range.

The carrier density change under low level injection is shown in Fig. 4.1(b). According to Section 2.2, an increase in carrier density causes a blueshift of the laser frequency. When the laser is locked on the positive frequency side, the carrier density increases, which then leads to a blueshift of the slave laser's cavity resonance frequency. The slave laser is thus shifted towards the master laser frequency and the locking range is increased. On the negative side, the carrier density decreases, which leads to a redshift of the slave's cavity resonance frequency, i.e., the slave gets tuned towards the master. This process yields the additional factor of $\sqrt{1+\alpha^2}$ in the expression for the locking range.

[2] E_i is the field that is 'available' to the locking process inside the cavity. In real experiments the coupling of the injected field to the cavity mode is difficult to determine.

Note that the above formula is generally valid only for weak injection. At higher injection rates, depending on the value of α, instabilities arise which alter the shape of the stable locking range. Examples on this are shown in the next section.

Equation (4.7) cannot, as such, be used to determine model parameters since the coupling of the injected field to the lasing mode is difficult to determine in experiments. In [94] it is shown that the change in the output power, or the carrier density, due to the injection is zero when $\Omega = \Omega_0 = \kappa$. This is illustrated in Fig. 4.1(b). The locking range is approximately between the maximum and minimum carrier excursions for $\alpha \gtrsim 3$. The LEF is then given by

$$\alpha = \sqrt{\left(\frac{\Delta\omega_{lb}}{2\Omega_0}\right)^2 - 1}. \tag{4.8}$$

This relation and a similar technique for the measurement of α is discussed in article **I**.

In semiconductors changes in carrier densities shift the quasi-Fermi levels, which in turn alter the voltage over the pn-junction. Therefore, carrier density changes can be detected by monitoring diode voltages. In experiments the peak voltage excursion in Fig. 4.1(b) tends to be less than the largest negative excursion (see, e.g., Fig. 4 in [**I**]). This has been studied experimentally in more detail in [95] and conjectured to be caused by instabilities arising from nearby complex dynamical states. The features outside the locking region in Fig. 4.1(b) are due to four-wave mixing effects and can be analysed analogously to that shown in the previous subsection [96, 97].

4.2 Large-Signal Regime

The orbit plot of Fig. 4.2(a) illustrates the complex dynamics that results when the injection rate is increased from the small signal regime. Here, local extrema of power time series have been plotted as a function of the normalised injection rate $K = \kappa\Omega_R^{-1}$ with the detuning kept constant at $\Omega = -\Omega_R$. In this simulation the laser parameters correspond to an edge-emitting semiconductor laser [**V**]. Starting from the left, the diagram shows a periodic orbit that bifurcates into a fixed-point solution at $K = 0.16$. The fixed point is stable only for a narrow range of K values. After the fixed point a periodic solution emerges followed by what appears to be a chaotic attractor at $K = 0.25$. There are many different chaotic attractors and periodic windows in the shown parameter range. On the right, a clear period-doubling cascade can be seen, the left side of which is connected to a chaotic attractor, and the right side is connected to a fixed point, i.e., the locked state (not shown).

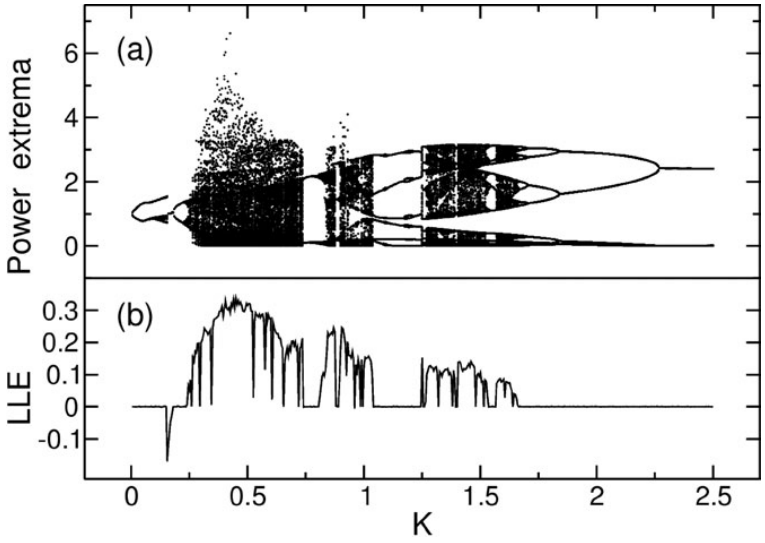

Fig. 4.2: Orbit diagram (a) and corresponding largest Lyapunov exponents (LLE) (b). Here K is the normalised injection rate $K = \kappa\Omega_R^{-1}$.

When the detuning is also allowed to change, solutions to the rate equations can be conveniently represented by drawing two dimensional maps, or diagrams, where regions of qualitatively different dynamical states are indicated. These maps are usually drawn with the injection rate on the x-axis and the frequency detuning on the y-axis. The rest of this chapter introduces numerical schemes that can be used to construct such stability maps, and in the next chapter experimental techniques are reviewed. The various different methods for producing mappings of the dynamics, both numerical and experimental, aid in the basic research of the behaviour of low-dimensional nonlinear systems and assist in locating a specific type of orbit to be used in applications.

4.2.1 Numerical Integration

A straightforward method to construct a map of laser dynamics is to integrate the rate equations for a large number of (K, Ω)-pairs and to manually classify the states using intensity time series, optical and power spectra, and perhaps Poincaré sections. This resembles the traditional experimental techniques but is very time consuming if detailed mappings are desired. A faster approach is to compute a single representative quantity from each time series and to plot a map based on it.

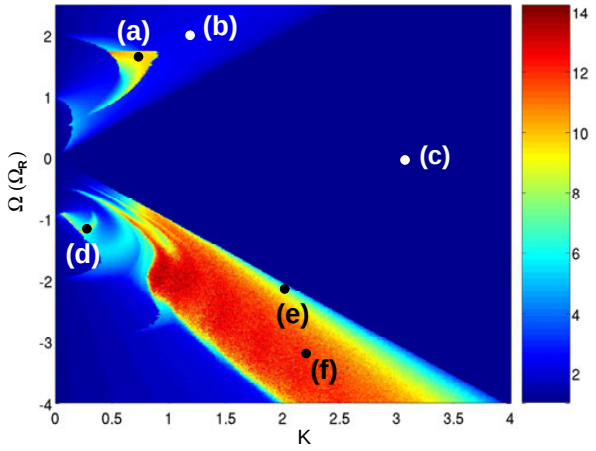

Fig. 4.3: Peak power in the Nd:YVO_4 laser subjected to optical injection. Power time series at the labelled points have been plotted in Fig. 4.4. Parameters as follows: $\tilde{J} = 2.5$, $\gamma_c = 1.74 \cdot 10^{10}\text{s}^{-1}$, $\gamma_s = 11100\text{s}^{-1}$, $\gamma_n = 27750\text{s}^{-1}$, $\gamma_p = 3.0 \cdot 10^5\text{s}^{-1}$, $\alpha = 0.2$, and $\beta = 0$.

In article **IV** such an approach was used when the dynamics of an Nd:YVO_4 laser subjected to optical injection was experimentally mapped. In that paper the quantity chosen was simply the peak power, which equals the maximum of local extrema. Consequently, the peak power corresponds to the envelope of Fig. 4.2(a). This quantity cannot, of course, as such reveal the nature of the state the laser is in (steady state, periodic orbit, ...), but it is reasonable to assume that the peak power will generally vary from state to state. Hence changes in the peak power give information on changes in the state of the laser. This is particularly true for slow inversion lasers, such as the Nd:YVO_4, which have a tendency for spiking. In Fig. 4.3 numerically obtained peak power relative to the free-running power is plotted. Power time series found at the labelled points have been plotted in Fig. 4.4. Here spontaneous emission noise must be taken into account, since noise reduces the peak powers of high power peaks considerably. Without amplitude noise peak powers in excess of 40 times the free-running power would occur at large negative detunings in Fig. 4.3.

In large parts of the (K, Ω)-plane multiple stable attractors exist. Which of these are found depends entirely on the initial conditions. Figure 4.3 was produced by increasing K from zero to $K = 4$ with fixed Ω. For a certain K_i, the initial condition was taken as the last computed phase point for the prior K_{i-1} integration. This procedure mimics experiments where the injection rate is ramped up from zero while the detuning is kept constant.

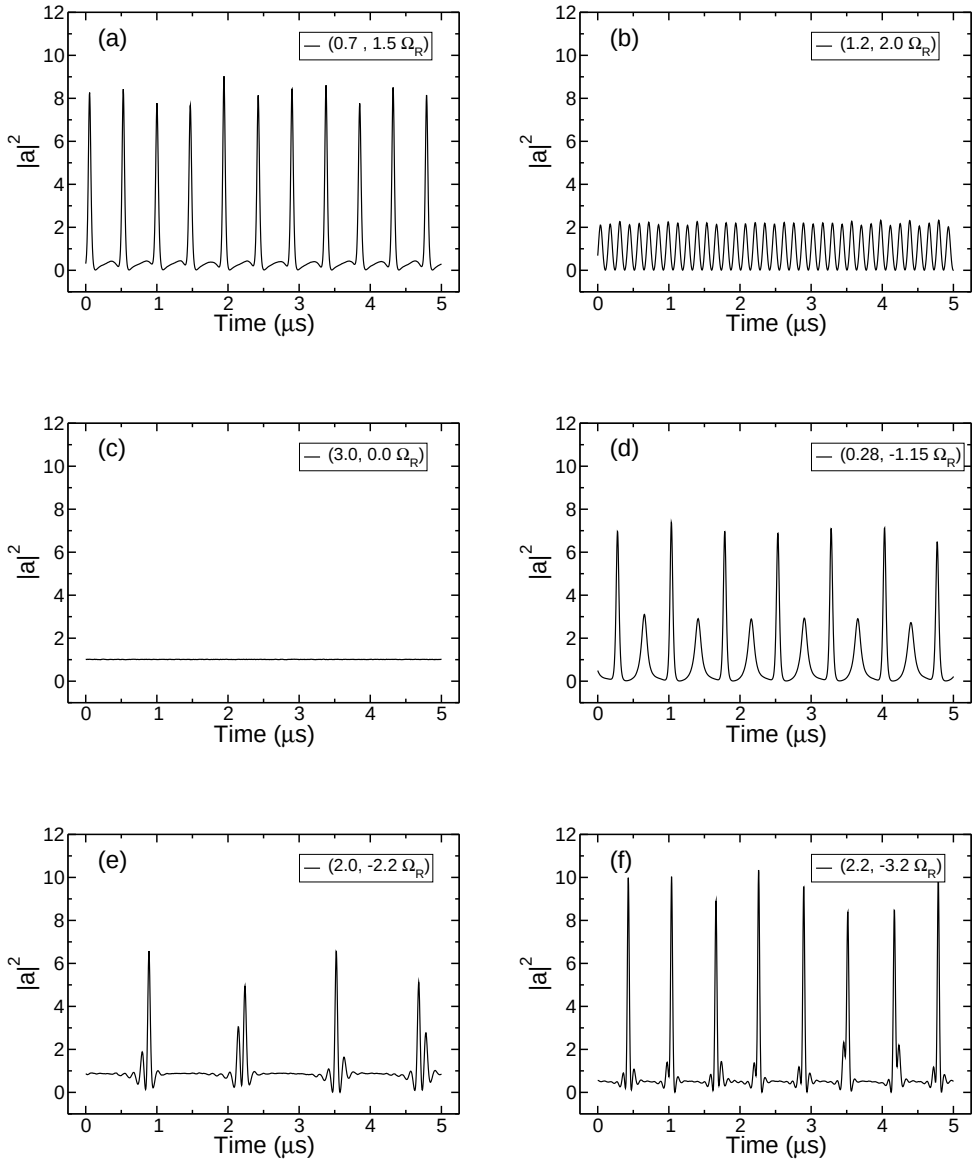

Fig. 4.4: Power traces corresponding to the labelled points in Fig. 4.3: (a) period-doubled limit cycle; (b) limit cycle before the Hopf transition to locking; (c) fixed point (locked); (d) limit cycle (on a torus); (e) limit cycle near the saddle-node transition to locking; (f) limit cycle.

The simple approach introduced here gives an overview of when and what is happening with the laser, and when compared to experimental results in Section 5.1, it gives an estimate for α.

4.2.2 The Largest Lyapunov Exponent

If the region of interest in the parameter plane contains locked, periodic and chaotic states, then the computation of the Largest Lyapunov Exponent (LLE) is a convenient way to get an overview of laser behaviour [98].

A negative LLE indicates a fixed point, i.e., locking in this case, and a positive LLE indicates chaotic states. The LLE is zero for periodic and quasi-periodic (torus) states. The absolute value of the LLE quantifies the stability of fixed points and the amount of chaos in chaotic attractors and it allows periodic windows inside chaotic islands to be mapped. Let

$$\frac{\mathrm{d}x}{\mathrm{d}t} = f(x) \tag{4.9}$$

be an m-dimensional autonomous dynamical system with a solution $x(t)$. Furthermore, let δt be the integration time step and introduce a small perturbation δx_0 to the system at $t = 0$. The linearised equation for the evolution of the perturbation is

$$\frac{\mathrm{d}\delta x}{\mathrm{d}t} = J(x)\delta x \tag{4.10}$$

where $J(x)$ is the Jacobian of the system. During the first time step δx_0 will evolve to

$$\delta x_1 = \delta x_0 e^{J(x_0)\delta t}. \tag{4.11}$$

After k time steps, the perturbation is given by

$$\delta x_k = \delta x_0 \exp(\sum_{l=1}^{l=k} J(x_l)\delta t) = \delta x_0 e^{\Lambda_k t_k} \tag{4.12}$$

where

$$\Lambda_k = \frac{1}{k}\sum_{l=1}^{l=k} J(x_l) \quad \text{and} \quad t_k = k\delta t. \tag{4.13}$$

The Lyapunov exponents λ_i are then defined as the eigenvalues of

$$\Lambda = \lim_{k\to\infty} \Lambda_k. \tag{4.14}$$

The number of Lyapunov exponents thus equals the dimensionality of the system. For simplicity, assume that all the eigenvalues of Λ are distinct. In that case there

is a matrix S such that $D = S^{-1}\Lambda S$ is diagonal with the eigenvalues of Λ as the diagonal elements. Equation (4.12) can then, in the limit $k \to \infty$, be written as

$$\delta x = SS^{-1}e^{\Lambda t}SS^{-1}\delta x_0 = Se^{Dt}S^{-1}\delta x_0. \tag{4.15}$$

Finally, defining $\delta y = S^{-1}\delta x$ and $\delta y_0 = S^{-1}\delta x_0$ yields

$$\delta y^{(i)} = e^{\lambda_i t} y_0^{(i)}, i = 1... \ m \tag{4.16}$$

for the components of y.

If at least one $\lambda_i > 0$, then a small perturbation of the trajectory will grow exponentially, i.e., there is sensitive dependence on the initial condition, which is the hallmark of chaos. On the other hand, if all $\lambda_i < 0$, then all directions are converging, i.e., the attractor is a fixed point. For a trajectory not containing a fixed point, at least one of the λ_i's is zero [99]. This is due to the fact that in the direction of the trajectory a perturbation neither shrinks nor expands on average.

Now consider a trajectory with initial condition $x(0) = x_0$ as well as a nearby perturbed trajectory with the initial condition $x(0) = x_0 + \delta x_0$. When these two trajectories are integrated in concert, the perturbed phase point will quite quickly align itself along the fastest growing direction relative to the unperturbed trajectory. As a consequence, the largest Lyapunov exponent (LLE) can be computed from the relation $d(t) = d_0 e^{\lambda_{LLE} t}$ where $d(t)$ is the separation between the phase points. For large $t = k\delta t$,

$$\begin{aligned}
\lambda_{LLE} &= \frac{1}{t}\ln\left(\frac{d(t)}{d_0}\right) \\
&\simeq \frac{1}{k\delta t}\ln\left(\frac{d_0 e^{\lambda_1 \delta t} e^{\lambda_2 \delta t} \dots e^{\lambda_k \delta t}}{d_0}\right) \\
&= \frac{1}{k}\sum_{i=1}^{k}\lambda_i, \text{ where } \lambda_i = \frac{1}{\delta t}\ln\left(\frac{d_i}{d_{i-1}}\right).
\end{aligned} \tag{4.17}$$

In order to keep the perturbed trajectory close to the unperturbed one, the distance $d(t)$ is normalised to d_0 at each time step. Furthermore, d_0 should be chosen much smaller than the characteristic length scale, which is 1 in the laser model due to the normalisation. In article **V** $d_0 = 10^{-9}$ was used.

Figure 4.2(b) compares the LLE to the orbit diagram for fixed $\Omega = -\Omega_R$. Clearly, the LLE is positive where the power extrema structure is complicated and zero for periodic dynamics. Also, the LLE is negative in a narrow range where a fixed point can be found. Letting the detuning also vary and by colour coding the LLE a two-dimensional map of laser dynamics is obtained. Figure 4.5 shows the LLE computed for the edge-emitter in article **V**. The map shows three distinct chaotic islands (red), two of which contain clear periodic windows.

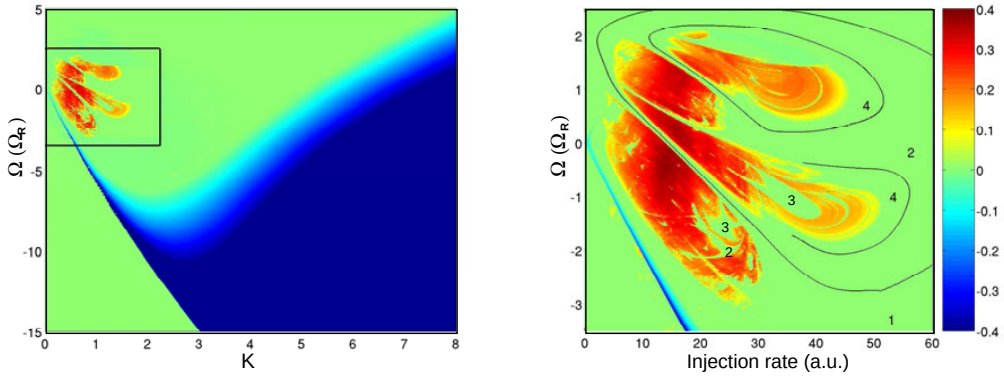

Fig. 4.5: The LLE of the edge-emitter studied in article **V** at a bias of $J = 1.25J_{th}$. The injection rate in the zoomed figure to the right has been scaled using the linear locking region boundary in order to fit the experimental map in Fig. 5.1. Parameters as follows; $\tilde{J} = 0.25$, $\gamma_c = 2.79 \cdot 10^{11}\text{s}^{-1}$, $\gamma_s = 1.06 \cdot 10^{9}\text{s}^{-1}$, $\gamma_n = 0.30 \cdot 10^{9}\text{s}^{-1}$, $\gamma_p = 1.04 \cdot 10^{9}\text{s}^{-1}$, $\alpha = 6.7$ and $\beta = 0$.

In most of the map $\lambda_{LLE} = 0$, which indicates periodic or quasi-periodic states (tori). The stable locking region (blue), where $\lambda_{LLE} < 0$, is considerably narrower than what might be expected based on Eq. (4.7), which is valid only for very small K.

4.2.3 Bifurcation Analysis

Section 4.2.1 presented a straightforward method for studying the dynamics of nonlinear systems. A less straightforward but much more powerful method is that of numerical bifurcation analysis. A bifurcation is a boundary between two regions of qualitatively different dynamics. Stability diagrams can be generated by first detecting a bifurcation somewhere in the (K,Ω)-plane and then numerically following this bifurcation. The stability map consists of a network of different types of bifurcation curves, each of which indicates a specific type of change in the dynamical state (see Fig. 6 in article **IV**).

Numerically, bifurcations of fixed points are detected by monitoring the (generalized) eigenvalues of the Jacobian matrix [100]. A bifurcation takes place when a single eigenvalue crosses the imaginary axis (saddle-node bifurcation) or when a pair of complex eigenvalues crosses the imaginary axis (Hopf bifurcation). In a saddle-node bifurcation, a saddle point and a node (stable or unstable fixed point) is born. In a Hopf bifurcation a fixed point bifurcates into a periodic orbit. The stability of the new solution depends on the other eigenvalues of the Jacobian. Bifurcations where attractors are born are called supercritical, whereas unstable

orbits are born in subcritical bifurcations.

Bifurcations of limit cycles are detected by constructing Poincaré maps P, also called stroboscopic or first-return maps, and then monitoring the eigenvalues of the Jacobian of P. In bifurcations of limit cycles, a saddle type periodic orbit and a stable or unstable periodic orbit is born in a saddle-node bifurcation of a limit cycle, which takes place when a single eigenvalue obtains the value +1. When a single eigenvalue obtains the value -1, a periodic orbit with twice the period is born in a period-doubling bifurcation. Finally, when the Jacobian of the map P acquires a pair of complex eigenvalues, a torus is born in a torus bifurcation (Hopf bifurcation of a limit cycle).

The bifurcations introduced above form the backbone of the bifurcation diagram of an optically injected laser [101]. There are several programme packages available that can be used to detect and follow the basic bifurcations introduced here. In article **IV** the package MATCONT [102] was utilised, which features an easy to use graphical user interface.

Routes to locking

The locked state corresponds to a fixed point of the rate equations. Fixed points are created and destroyed in Hopf and saddle-node bifurcations. Which of these form the boundary of the locked state depends on the laser parameters, α in particular, as well as on the injection rate and detuning [101]. When $\alpha > 0$, most of the upper locking boundary is formed by a Hopf bifurcation. The Hopf bifurcation is a smooth transition, since the oscillations are born with an amplitude proportional to $\sqrt{\xi}$ where ξ is a distance from the boundary [51]. This smoothness can be seen in Fig. 4.3, where the upper locking boundary barely shows up in the peak power mapping.

The saddle-node transition was already briefly discussed in Chapter 3 in connection with Adler's model for locking. For very small injection rates and detunings, this type of bifurcation bounds the locked state both from above and from below, and for larger injection rates it is only found at negative detunings. In the Nd:YVO_4 case, the saddle-node bifurcation takes place on a periodic orbit. When the boundary is approached from the limit cycle side, the phase point begins to spend more and more time in a certain part of the periodic orbit until it finally makes a complete stop. Other parts of the orbit are traversed with longer and longer delays. This process results in a power time series that consists of increasingly long delays between pulses, and can be seen as high peak powers near the lower locking boundary in Fig. 4.3 and Fig. 4.4(e). Spontaneous emission noise reduces the peak powers considerably. More detailed numerical and experimental power time series of an Nd:YVO_4 laser en route to locking can be found in [61].

In the edge-emitter of article **V**, saddle-node transitions to locking are smoother,

with pulse peak powers only somewhat larger than the free-running power. Furthermore, this type of behaviour can only be found under low level injection. At higher powers the fixed point disappear suddenly, with the laser making a transition to a nearby periodic orbit.

The Hopf and saddle-node bifurcations are the generic bifurcations that form the major parts of the locking boundaries. This is, however, not the whole story. For instance, at certain points these bifurcation curves collide and form saddle-node-Hopf bifurcations. The bifurcation structure and the route to locking is very complicated in the vicinity of such points [103, 104].

Routes to chaos

In Fig. 4.5 large regions of chaotic dynamics can be seen. The type of route to chaos taken by the slave laser depends on which direction the chaotic attractor is approached from [105]. Chaotic attractors can appear via several different routes [106]. In the period doubling route (Feigenbaum scenario) an attracting periodic orbit undergoes an infinite number of successive period doublings (as a parameter is varied) until it finally becomes chaotic. This route is clearly seen in Fig. 4.2(a) for $K \gtrsim 1.7$.

In an intermittent route (Pomeau-Manneville scenario) of type I, a periodic orbit loses its stability with the appearance of a chaotic attractor. The 'ghost' of the periodic orbit left behind leads to chaotic output interrupted by sequences of periodic behaviour. Hence the name intermittent. If the parameter is varied in the other direction, the chaotic attractor disappears when an attracting periodic orbit is born in a saddle-node bifurcation. Before this actually happens, the chaotic attractor begins to sense the periodic orbit about to form, which then leads to the characteristic sequence of chaotic output interrupted by longer and longer intervals of periodic behaviour. Other variations of the intermittent transition also exist (type II and type III).

In the Ruelle-Takens-Newhouse scenario, also called break-up of a torus, a fixed point undergoes three successive Hopf-bifurcations. In the first stage a periodic orbit is born. In the second stage the periodic orbit bifurcates into a torus in a torus bifurcation (Hopf bifurcation of a limit cycle). At the third Hopf bifurcation, a hypertorus is born; however, the hypertorus is usually unstable and a chaotic attractor appears instead. Motion on a torus can be quasi-periodic or locked[3] and this is governed by resonance tongues. In another version of the break-up of a torus route to chaos, a smooth transition to chaos appears where the resonance tongues begin to overlap.

If a chaotic attractor coexists with another attractor, then it can collide with the boundary between the basins of attractions of the two attractors. If this

[3] There is a periodic orbit on the torus.

happens, the chaotic attractor can disappear in what is called a boundary crisis. Chaotic attractors born via break-up of tori are usually much larger than those born via period-doubling cascades. However, a small attractor can suddenly increase in size when colliding with the stable manifold of an attractor of the saddle type [107]. Such a process is called an interior crisis.

A period-doubling route to chaos was first observed in a loss modulated CO_2 laser [85]. In an optically injected semiconductor laser somewhat clear experimental evidence for a period-doubling route to chaos was first given in [108], for an intermittent transition in [109], and for a quasi-periodic route, i.e., break-up of a torus, in [93].

The next chapter takes a closer look at how the dynamical complexity of coupled lasers can be experimentally investigated. Some applications for these systems are also presented.

5. OPTICAL INJECTION EXPERIMENTS

Unidirectionally coupled lasers have been studied since the 1960s [80]. However, most of published experimental work focus on isolated phenomena in the (K, Ω)-plane, whereas detailed global experimental mappings are scarce. For semiconductor lasers, detailed global mappings have been published in, e.g., [110, 109, 93] for DFB lasers and in [111] for VCSELs with orthogonally polarised injection. The most detailed experimental mappings to date have been performed on Fabry-Pérot type semiconductor lasers in [112] and [113]. These mappings are compared in detail to modelling results in article **V**. In article **IV** of this Thesis the global dynamics of an optically injected Nd:YVO_4 laser is experimentally mapped in detail for the first time.

Experimentally, the dynamical state of a laser can be deduced from optical spectra, power spectra, power time series, or combinations thereof. Which of these methods are applicable in practise depends on the type of laser under study. In order to obtain undistorted power time series of lasers during optical injection, the optical bandwidth of the detection system (photodetector and real-time oscilloscope) must be several times higher than the characteristic frequency of the slave laser. Consequently, semiconductor lasers require oscilloscopes with very high bandwidths. Such instruments are still very expensive, if available at all. Thus injection experiments with semiconductor devices must usually rely on optical and microwave spectra, although short time series can be obtained with streak cameras. Apart from potential applications, the high frequencies involved does give one advantage - the frequency stability of the lasers during experiments does not pose a problem.

In solid-state lasers it is the other way around. On one hand, the low characteristic frequencies of a few MHz mean that power time series can easily be measured with contemporary oscilloscopes and photodetectors. On the other hand, obtaining optical spectra with 100 kHz resolution is more of a challenge, especially when the long term frequency stability of the free-running lasers is an order of magnitude poorer. Problems with the frequency stability of the lasers can be avoided by performing the measurements fast enough, as discussed in Sec. 5.2.

In the next two sections experimental techniques used in optical injection experiments on semiconductor and Nd:YVO_4 lasers are discussed.

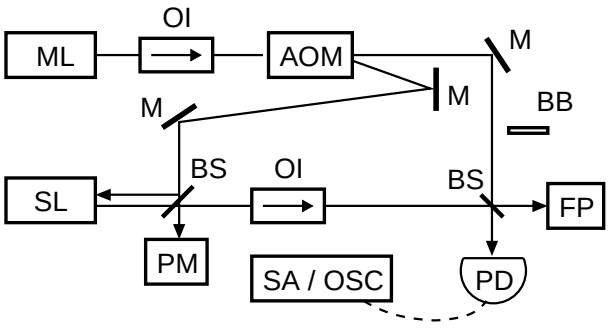

Fig. 5.1: A typical setup used in optical injection experiments with semiconductor lasers. ML: master laser; SL: slave laser; PM: power meter; OI: optical isolator; AOM: acousto-optic modulator; M: mirror; BS: beam splitter; BB: beam block; PD: fast photodetector; SA: microwave spectrum analyzer; OSC: oscilloscope; FP: Fabry-Pérot interferometer.

5.1 Semiconductor Lasers

A typical experimental setup is shown in Fig. 5.1. Light from the master laser (ML) is directed towards the cavity of the slave laser (SL) via an optical isolator (OI) and an acousto-optic modulator (AOM). The isolator prevents optical feedback to the ML and ensures that the coupling is unidirectional. Optical spectra are measured with a Fabry-Pérot interferometer (FP). A fast photodiode (PD) coupled to a microwave spectrum analyser (SA) gives the power spectrum, and the power meter (PM) measures the relative amount of injected light.

A convenient way of studying the dynamics is to have a computer control the experiment; that is, to increase the amount of injected light and to continuously record optical and microwave spectra. The spectra can then be colour coded and plotted next to each other to yield a pseudo-colour plot of the events taking place as the injection rate is varied [114, 112]. Figure 5.2 shows examples of such plots for a 690-nm EEL [115]. The injection rate increases from left to right and each vertical column represents the colour coded optical (a) and microwave spectrum (b) at the corresponding injection rate. Note that, in this case, the photodetector PD had an electrical bandwidth of only 1 GHz, which explains the limited power at the highest shown frequencies in the chaotic regions in Fig. 5.2(b).

Starting from left, the spectra correspond to Adler type frequency pulling ($\zeta < 0.02$ where ζ is the injection rate), followed by a narrow range of locking, then a limit cycle ($0.05 < \zeta < 0.1$), chaos, a periodic orbit ($0.18 < \zeta < 0.2$), then chaos again followed by a periodic orbit that eventually bifurcates back to the locked state at the far right (via a Hopf bifurcation). By taking several such sweeps with different detunings a map of the dynamics can be put together, as

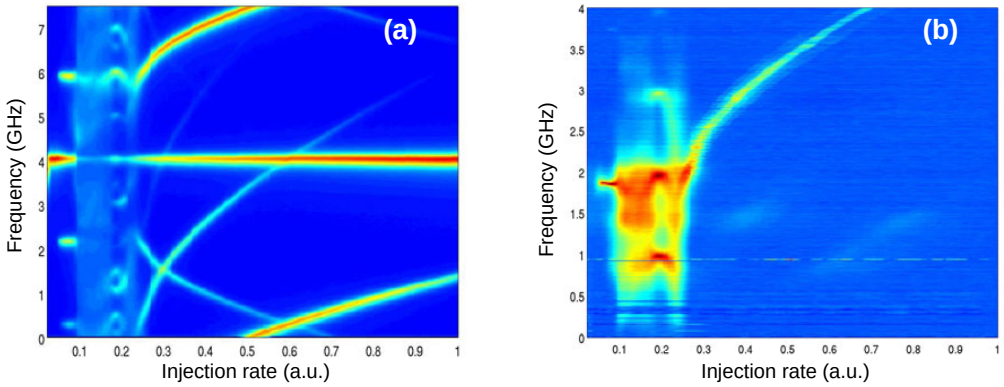

Fig. 5.2: Pseudo-colour plots of optical (a) and microwave (b) spectra of an EEL subjected to optical injection (logarithmic colour scales). In (b) the electrical bandwidth of the photodetector was only 1 GHz, which explains the low powers at the highest frequencies in the chaotic regions. The absence of power at some of the low frequencies is an artifact.

done in [112, 113] for an edge-emitter operating around 634 nm. The results of these mappings, one of which is reproduced with permission in Fig. 5.3, compare well with the numerical simulations in Fig. 4.5 and article **V**. The periodic orbits (1,2,3,4) in the experiment are in good agreement with those in Fig. 4.5, as are the chaotic islands (C) although the chaotic islands in the simulation are a bit larger. This could be due to the neglect of spontaneous emission, which is known to cause extra damping of instabilities in strongly modulated semiconductor lasers [116, 117]. In the regions marked 'OM' the laser has made a mode hop to another nearby longitudinal mode. These features can be taken into account by adding an equation for a nonresonant mode into the model [93]. In such models power is transferred to the nonresonant mode mostly near the locking range, in agreement with that seen in Fig. 5.3. To avoid these mode hops a DFB laser with increased side-mode suppression should be used.

5.2 Nd:YVO_4 Solid-State Lasers

The low characteristic frequencies of slow inversion lasers, such as Nd:YVO_4 lasers, means that power time series can be easily recorded, whereas optical spectra are more difficult to measure. The low characteristic frequencies also imply that the frequency stability of these lasers becomes a problem, since the detuning between the lasers must stay constant during a sweep of the injection power. The stability must be at least an order of magnitude smaller than the relaxation

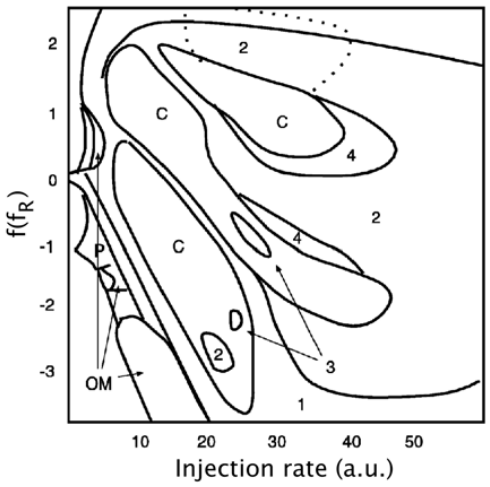

Fig. 5.3: Experimental mapping of the dynamics of an 634-nm EEL. Reproduced from [113] with permission from the publisher. C: chaos; 1,2,3 and 4: periodic orbits of different periodicity; OM: other longitudinal modes; P: frequency pulling.

oscillation frequency, which means $\mathcal{O}(100$ kHz) in this case. Such a long term stability is difficult, if not impossible, to achieve, considering that no active stabilisation methods can be allowed. The solution is to ramp up the injection rate quickly so that the detuning does not have time to drift. A lower boundary for the sweep time is set by the requirement that the injection power increase must be adiabatic, meaning that it can be considered constant at each power level. On the left in Fig. 5.4 is a power time series recorded with an oscilloscope while the injection power is ramped up from zero until locking is reached in roughly one millisecond [**IV**]. This trace contains about 10^5 data points and all dynamical states the laser goes through on its route to locking. As an example, the inset shows a clear period-doubling bifurcation at $t = 0.33$ ms.

An overview of laser response to injection as a function of detuning and injection rate can be obtained by colour coding the peak power, as discussed in Sec. 4.2.1. Such a plot is shown on the right in Fig. 5.4. This map reveals clear asymmetry with respect to the detuning and is in good agreement with the numerical map in Fig. 4.3 if $\alpha \approx 0.2...\ 0.3$. Individual power time series from different parts of the map can also be compared and they too demonstrate a remarkable agreement between the model and the experiment [**IV**][61]. In article **III**, the above estimate for α is confirmed using an independent FM/AM technique. Prior to these results, the LEF in solid-state lasers was usually assumed to be very small, although in [118] evidence was given for $\alpha \approx 1$ in a Nd:YAG microchip laser.

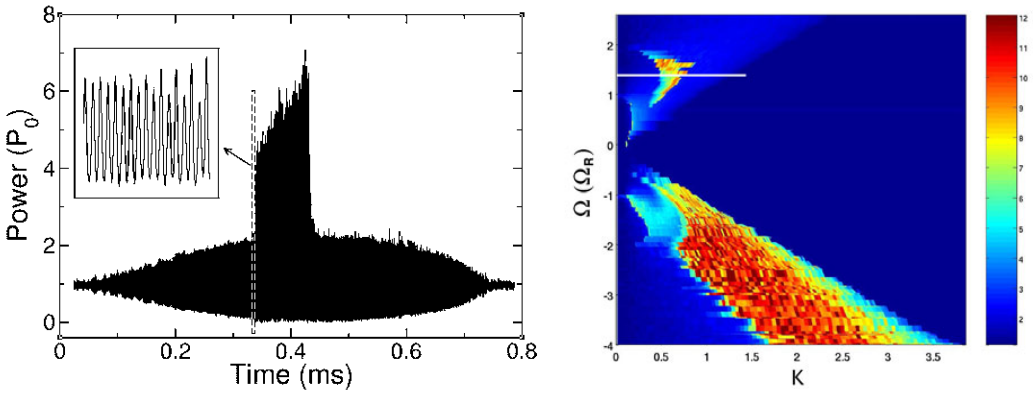

Fig. 5.4: An example of a power time series measured during a sweep of the injection rate for fixed detuning $\Omega = 1.4\Omega_R$ (left). The inset shows a clear period-doubling bifurcation. Several traces can be combined into a map by colour coding the peak power (right). The white line indicates the position of the trace shown on the left.

Such a large value seemed to agree with [119], where $\alpha = 1$ and $\alpha = 2$ were used when feedback experiments on Nd:YVO_4 lasers were modelled. However, based only on the symmetrical locking region in Fig. 5.4, $\alpha \lesssim 0.4$ must hold.

For a more detailed account of what kind of dynamics is contained in the recorded traces, all traces should be analysed individually. One way of doing this is to manually go through the data, trace by trace, and to plot a map that shows where different dynamics was found. Another, more efficient, way is to let a computer go through the traces looking for signs of different bifurcations. For example, a period-doubling bifurcation corresponds to a situation where the time between subsequent power maxima is doubled. Such an approach is presented in [120]. The presence of a significant amount of noise complicates the seemingly straightforward approach.

5.3 Applications

The research on optical injection as well as on other types of coupled laser systems is motivated by the many present as well as several potential future applications of these systems. To conclude the introductory part of this Thesis, some applications are presented where optical injection and optical feedback can be used to advantage. Most traditional applications use the locked or low injection regimes, but recently, potential applications for the periodic states, and the chaotic states in particular, have been proposed. A particular state of a laser can only be used

in applications if it can be found in the parameter space. To this end, the different types of stability maps drawn in this and in the previous chapter come in handy.

5.3.1 Basic Research

Model systems: A multitude of synchronisation phenomena and other types of nonlinear processes are encountered in nature. However, systematic experimental studies of these dynamical systems are often complicated by the limited external control that can be applied as well as by the long time scales. An optically injected class-B laser represents a low-dimensional dynamical system with two relatively easily controllable parameters – the frequency detuning and the injection rate – and can, therefore, together with the rate equations serve as models for research on the dynamics of nonlinear low-dimensional systems. Analogously, lasers with optical or opto-electronic feedback can serve as models for delay coupled dynamical systems. The two control parameters in those cases are the delay time and the coupling strength, both of which are easily accessible quantities.

Laser characterisation: Optical injection and optical feedback can be used to advantage in laser characterisation. In Section 4.1 and in article **II** amplification of a weak injected probe as a function of detuning was measured to obtain information on the relaxation oscillation frequency and the damping rate. In article **I** several methods based on optical injection and optical feedback were applied to measure the linewidth enhancement factor α.

Light amplification: Sometimes low power laser light of good quality needs to be amplified while maintaining its properties. One way of achieving this is to injection lock a more powerful laser to this light. The slave laser will then inherit the frequency of the injected light while providing amplification of several orders of magnitude. For example, in a frequency comb the power in a single line is very small, $\mathcal{O}(1\ \mu\mathrm{W})$, and in order to compare the frequency to, e.g., a 100 μW iodine-stabilised He-Ne laser, the light must be amplified in order to obtain a reliable beat frequency count. One way of achieving improved signal to noise ratio is to injection lock a semiconductor laser of a few tens of mW of average power to the comb line and to count the beat signal between the He-Ne and the semiconductor laser [121]. In the cited paper amplification of as much as 39 dB was demonstrated.

As a side note, in the early days of radio communications, powerful triode signal generators were injection locked to smaller but much more stable oscillators in order to realize stable high-power signals.

5.3.2 Telecom

Modulation bandwidth: The faster a laser can be modulated, the higher the achievable bitrates in telecommunication systems based on directly modulated lasers.

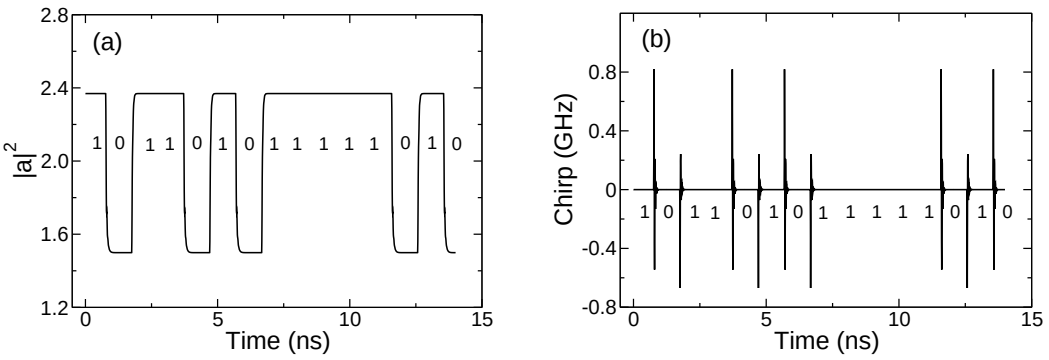

Fig. 5.5: A noiseless semiconductor laser ($f_R = 4.4$ GHz, $\alpha = 4$) under strong optical injection $(\Omega, K) = (0, 8)$ and modulated with an ideal 1 Gbit/s NRZ pseudo-random sequence: (a) amplitude modulation and (b) frequency chirping.

An interesting discovery is that the modulation bandwidth of a laser can be increased by strong optical injection [122]. Recently, a small signal modulation bandwidth of 50 GHz was demonstrated in a 1.55 μm multi-quantum-well VCSEL [123] with a free-running relaxation oscillation frequency of 7 GHz. In [124] the bandwidth of a quantum-dot VCSEL was raised from 1.8 GHz to 7.4 GHz. The increase has been attributed to pulsations of the intracavity field and population inversion at frequencies determined by the frequency detuning between the master and the slave laser [125]. Another advantage with this technique is that frequency chirping is also reduced. Figure 5.5 shows the same situation as Fig. 2.7, i.e., a VCSEL modulated with an ideal 1 Gbit/s NRZ pseudo-random sequence, but now strong optical injection is also applied. Note the improved bit pattern and the reduction in chirp.

Carrier generation: In future radio-over-fibre applications, microwave signals will be transported optically to local base stations which receive the signals and transmit them via microwaves to the surroundings. In [126] a method is presented for producing a high frequency microwave carrier riding on light from a semiconductor laser. In that scheme an optically injected laser is driven into limit cycle dynamics (region '1' in Fig. 4.5). To reduce the jitter of the generated wave, the slave laser is double-locked by applying a small microwave signal to the bias of the slave. Up to 14-GHz signals with excellent stability were successfully produced. The direct small-signal modulation bandwidth of the laser was limited to only 3 GHz due to device parasitics. In [127] the same period-1 state is used to generate nearly single-sideband frequency modulated communications signals.

Frequency division: Frequency division is an important element in communications systems, e.g., in optical time division multiplexing. In [128] the frequency doubled solution (region '2' in Fig. 4.5) is utilised to frequency double or divide a

microwave carrier. Frequency multiplication is achieved when the laser dynamics is double-locked to a microwave signal at the subharmonic frequency. Conversely, frequency division is realised when the slave laser is double-locked to a microwave signal at the primary frequency.

Secure communication: In recent years, the possibility of realising high-speed secure communication systems using chaotic optical carriers has raised considerable interest [129]. In the simplest scheme, known as chaos masking (CMA), a chaotic carrier in the transmitter laser is generated with optical injection, or feedback, and a message is added to this carrier by, e.g., modulating the current of the slave laser or by modulating the light to be transmitted with an external modulator. In the receiver end, one part of the incoming light is injected into the receiver laser, which, if conditions are right, synchronises to the injected light. The receiver laser acts as a chaos-pass filter that reproduces the chaotic fluctuations of the transmitter laser but suppresses additional encoded signals [130]. The message is then recovered by subtracting the receiver output from the original signal. The feasibility of such a scheme was first numerically demonstrated in [131], where two solid-state lasers were used two transmit a 100 kbit/s bit sequence. In current state-of-the-art setups based on semiconductor lasers signals of several GHz are routinely transmitted. In [132] a composite TV-signal at a carrier frequency of 2.4 GHz was encoded and successfully received, although the received image quality was less than perfect.

5.3.3 Other Areas

Chaotic radars: Conventional pulsed radars send out short microwave pulses and record the time it takes for the reflected waves to return. Distance is then computed from the time delay. A random signal radar (RSR) sends one part of a random microwave train towards the target and keeps one part as a reference. When the reflected wave train returns it is autocorrelated with the reference. Since the wave train is random, the autocorrelation function has a large value only for a certain time delay, which corresponds to the round-trip time. Typical electrical noise circuits and chaotic circuits have bandwidths below 1 GHz. In [133] an RSR that utilises the broadband chaotic signal ($\gtrsim$ 10 GHz) from an optically injected semiconductor laser was proposed and demonstrated. According to the authors of the cited paper, their technique offers improved range resolution compared to conventional radars, and it reduces the need for sophisticated microwave electronics.

Interferometry: Important areas of application of optical feedback are displacement measurement and velocimetry. The conventional way of optically measuring displacement (velocity) is to construct a Michelson interferometer and to simply count the resulting fringes (beat frequency). A more exotic approach is

the self-mixing scheme, where laser light reflected from the target is fed back into the cavity of the emitting laser and the resulting changes in the laser output power are monitored [89]. The signal to noise ratio is not as good as what can be achieved with the conventional interferometers, but due to its simplicity, the self-mixing scheme is a very cost-effective way of realising sensitive sub-wavelength detection. Additionally, the presence of the LEF in semiconductor lasers leads to an asymmetry with respect to the target movement, which means that the direction of movement can also be deduced (see Fig. 7(a) in article **I**).

This discussion on a few selected applications brings the introductory part of this Thesis to an end. The list presented above is by no means exhaustive. Especially in the field of telecommunications several other uses for optical injection have been proposed, including wavelength conversion (e.g. [134]), clock recovery (e.g. [135]) and optical phase-locked loops [136]. The next chapter summarizes the results of this work and gives a brief outlook.

6. CONCLUDING REMARKS

In conclusion, the first part of this Thesis reviewed the historical milestones that led to the contemporary semiconductor and Nd:YVO_4 lasers studied in this work. Basic properties of class-B lasers were reviewed using a simple but powerful rate-equation model. Model parameters and solitary laser dynamics were discussed with an emphasis on the linewidth enhancement factor α and on artificially or noise induced dynamics around the steady state. The second part of this Thesis focused on the dynamics of unidirectionally coupled lasers. Weak optical injection was shown to be useful in model parameter extraction, whereas strong optical injection was shown to induce a wealth of interesting and potentially useful complex nonlinear dynamics.

In particular, this work presented (i) the first systematic comparison between many different α-measurement techniques. A need for such a work was noted already in the late 1980s in a review paper by Osiński and Buus [49]. Since then, a number of new techniques have been presented but still a comprehensive comparison between the various techniques have been lacking. In this Thesis the first step towards a correction of this situation was taken.

(ii) A nonmonotonous linewidth behaviour at threshold in a VCSEL was reported on for the first time. The effect, which was predicted theoretically in [67], has previously been observed only in DFB lasers. These new results show that the effect can be expected in many types of lasers with a strong coupling between the gain and the refractive index.

(iii) A variation of an experimental technique originally introduced by Harder *et al.* [73] was put forward to directly measure the linewidth enhancement factor in a microchip solid-state laser for the first time. The result $\alpha = 0.25 \pm 0.13$ confirmed the estimates of $\alpha = 0.2...0.3$ obtained indirectly from optical injection experiments.

(iv) A novel and powerful experimental technique for studying the dynamics of coupled microchip solid-state lasers was presented. The method is based on continuous power time series measurements during sweeps of the injection rate. By rapidly driving the injection rate up and down, the frequency instabilities of these types of lasers (relative to their characteristic frequency) are avoided. Inherent to the method is that all the dynamical states the slave laser goes through on its way to locking are automatically recorded.

(v) Finally, detailed previously published experimental mappings of the dynamics of an optically injected semiconductor laser were compared to the rate-equation model by computing the largest Lyapunov exponent. The results show that in order to reach at a quantitative agreement between experiment and theory, the value of the linewidth enhancement factor must be increased from the earlier reported value of 3.9 to about 6.7. The results also show that the nonlinear gain rate γ_p should not be neglected.

6.1 Outlook

From a pure dynamics point of view, the most important parameter in semiconductor lasers is the linewidth enhancement factor α, which influences many of the basic properties of free-running and pump-modulated lasers, as well as the basic properties of lasers with a coupling to an external field, cavity or reflector. The effect of the other parameters is mostly to determine the time scale via the relaxation oscillation frequency. A nonzero α arises due to an asymmetric gain profile or due to a detuning from the gain peak in the case of a symmetric gain profile. In semiconductor lasers the gain profile is highly asymmetric, which results in a large α-factor even when the cavity allows lasing at or near the gain peak, as is the case in edge-emitters.

The measurements on the Nd:YVO_4 lasers presented in this work left the physical origin of α unknown. By combining these experiments with spontaneous emission measurements that allow the gain profile to be studied, the origin of α could probably be determined. Furthermore, if the 1-mm crystals were exchanged to shorter ones, say 0.5 mm, and equipped with an external movable mirror, then the oscillation frequency of the slave laser could be tuned mechanically. It would then be possible to measure α and to study the injection induced dynamics as a function of the frequency detuning from the gain peak. Another advantage of changing the crystals to shorter ones would be the resulting increase in the relaxation oscillation frequency f_R. An increase in f_R means that the relative frequency stability is improved. The relaxation oscillation frequency is a function of the cavity round-trip time, and when the round-trip time is decreased, f_R is increased. Furthermore, 0.5-mm crystals usually come with 3% neodymium doping. The increased doping level shortens the upper state lifetime and increases γ_s and γ_n by a factor of three [137], which in turn causes an additional increase in f_R.

The experimental data on the optically injected Nd:YVO_4 laser is in surprisingly good agreement with the rate-equation model considering the amount of noise present and the frequency instabilities between the master and the slave laser, which forced the measurements to be performed quickly. Due to the frequency instabilities, it is unlikely that the unidirectionally coupled solid-state

laser system will find any applications in the future, besides those of a more academic nature. This is in contrast to semiconductor lasers with optical injection, where the high characteristic frequencies mean that frequency stability is not a problem, except perhaps over long time scales. If coupled semiconductor lasers are to be used in commercial applications, methods must be found by which the injection parameters can be stabilised over long time scales. Otherwise, the injection rates and, in particular, the detuning between the lasers will drift, making the systems unreliable and of little practical use. A potential solution is to manufacture monolithic chips containing two identical lasers. In that case both lasers will feel similar changes in their environment and will drift in concert maintaining a constant detuning. If more precise control is needed, e.g., to counter drifts due to ageing, methods for active stabilisation of the injection parameters must be found.

From a nonlinear dynamics point of view, an ideal laser system to study would be one with relaxation oscillations around a few hundred MHz. This would mean that (i) contemporary oscilloscopes and photodetectors would have no problem in keeping up with changes in the outputs of the lasers, (ii) optical spectra could be directly measured with Fabry-Pérot interferometers, and (iii) frequency stability would not be a problem. With such a system the experimenter would be getting the best of both the semiconductor and the solid-state laser worlds – good frequency stability and low frequencies. Such a system could potentially be constructed using vertical external-cavity semiconductor lasers (VECSELs) or external cavity EELs.

Dynamics in coupled lasers is currently an active field of research motivated by the controllable complex nonlinear dynamics and by several potential future applications. With the results presented in this Thesis, the author hopes to have made a contribution to the advancement of this particular sub-field of laser physics.

ERRATA

IV: The Langevin field noise spectral density D_a^2 is defined by $D_a^2 = \frac{1}{2}\langle F_a(\omega) F_a^*(\omega)\rangle$.

V: Eq. (7) should read $\frac{I_{MP}}{I_{SB\mp}} = ...$ Furthermore $\Delta = \arg(1+ix)$ and hence $\Delta = 0$ if $\alpha = \beta$ or $\Omega_M \gg \gamma_p$.

ACKNOWLEDGEMENTS

This work has been carried out at the Accelerator Laboratory of the Department of Physical Sciences, University of Helsinki. Thanks are due to the head of the department, Prof. Juhani Keinonen, to the current and former heads of the Accelerator Laboratory, Prof. Jyrki Räisänen and Doc. Eero Rauhala, and to all others involved in keeping the department, its buildings, laboratories, classrooms and computers up and running. Thank you.

The author's interest towards laser physics arose from the lectures of Doc. Birger Ståhlberg, and from the remarkable performance and elegance of iodine-stabilised He-Ne lasers. During experiments, the author has benefited a great deal from Birger's expertise with laboratory apparatus.

The author is grateful to Thesis supervisor Doc. Åsa Lindberg for providing the opportunity to work in the exciting field of laser physics. Åsa's critical comments on manuscripts have improved the quality of this work considerably.

Fellow graduate student, M.Sc. Simo Valling, is recognised for the many hours of laboratory work needed to obtain data on Nd:YVO_4 laser dynamics. The author is also thankful for the many discussions and for the pleasant company to several summer schools and conferences in Finland and abroad.

Prof. Zeno Toffano (Supélec, France) is acknowledged for bringing the threshold transition and its dependence on the linewidth enhancement factor to the authors attention, and for the fruitful collaboration over the Internet.

Ph.D. Stefan Eriksson is acknowledged for showing the ropes in the very early stages of this work.

Marja-Liisa Louhio is acknowledged for the kind assistance when problems with "työsopimus", "matkamääräys" and the occasional "matkalasku" arose.

A nice end to many a work filled week has been the Friday afternoon floorball session. Good game guys.

This Thesis could not have been completed without financial support from Magnus Ehrnrooth Foundation. Furthermore, financial support and encouragement from Ruth och Nils-Erik Stenbäcks stiftelse, Kulturfonden, The Finnish Academy of Science and Letters, Vilho, Yrjö and Kalle Väisälä Foundation, Svensk-österbottniska samfundet and Vasa nation is gratefully acknowledged.

These pages are dedicated to Lisa for her contributions to the more important things in life.

In Helsinki, January 2007,

Thomas Fordell

BIBLIOGRAPHY

[1] H. Kragh, "Max Planck: the reluctant revolutionary", *Physics World*, vol. 13, no. 12, pp. 31-35, 2000

[2] A. Einstein, "Zur Quantentheorie der strahlung" (On the quantum theory of radiation), *Physika Zeitshrift*, vol 18, pp. 121-128, 1917

[3] An english translation of [2] has been published in H.A. Boorse, L. Motz (Eds.), *The world of the atom*, Volume II, Basic Books, 1966, pp. 884-901

[4] R. Friedberg, "Einstein and stimulated emission: A completely corpuscular treatment of momentum balance", *Am. J. Phys.*, vol. 62, no. 1, pp. 27-32, 1994

[5] C.H. Townes, *How the laser happened*, Oxford University Press, 1999

[6] A.L. Schawlow, C.H. Townes, "Infrared and optical masers", *Phys. Rev.*, vol. 112, no. 6-15, pp. 1940-1949, 1958

[7] T. Maiman, "Stimulated optical radiation in Ruby", *Nature*, vol 187, pp. 493-494, 1960

[8] J.L. Bromberg, "The birth of the laser", *Physics Today*, vol. 41, no. 10, pp. 26-33, 1988

[9] A. Javan, W.R. Bennett Jr., D.R. Herriott, "Population inversion and continuous optical maser oscillation in a gas discharge containing a He-Ne mixture", *Phys. Rev. Lett.*, vol. 6, no. 3, pp. 106-110, 1961

[10] R.D. Dupuis, "An introduction to the development of the semiconductor laser", *IEEE J. Quantum Electron.*, vol. 23, no. 6, pp. 651-657, 1987

[11] Z.I. Alferov, "Nobel lecture: The double heterostructure concept and its applications in physics, electronics, and technology", *Rev. Mod. Phys.*, vol 73, no. 3, pp. 767-782, 2001

[12] K. Uehara, K. Katukua, "New method of frequency stabilization of semiconductor lasers", *Jpn. J. Appl. Phys.*, vol. 27, no. 2, pp. L244-L246, 1988

[13] H. Ludvigsen, C. Holmlund, E. Ikonen, M.-L. Junttila, "Frequency stabilization of a GaAlAs semiconductor laser by voltage control", *Appl. Opt.*, vol. 31, no. 8, pp. 2284-3386, 1992

[14] H. Ludvigsen, C. Holmlund, E. Ikonen, "Heterodyne frequency measurement of a voltage-controlled diode laser", *IEEE Trans. Instrum. Meas.*, vol. 42, no. 2, pp. 426-429, 1993

[15] I. Melngailis, "Longitudinal injection-plasma laser of InSb", *Appl. Phys. Lett.*, vol. 6, no. 3, pp. 59-60, 1965

[16] H. Soda, K. Iga, C. Kitahara, Y. Suematsu, "GaInAsP/InP surface emitting injection lasers", *Jpn. J. Appl. Phys.*, vol. 18, no. 12, pp. 2329-2330, 1979

[17] F. Koyama, S. Kinoshita, K. Iga, "Room-temperature continous wave lasing characteristics of a GaAs vertical cavity surface-emitting laser", *Appl. Phys. Lett.*, vol. 55, no. 3, pp. 221-222, 1989

[18] K. Iga, "Surface emitting laser - Its birth and generation of new optoelectronics field", *Sel. Top. Quantum Electron.*, vol. 6, no. 6, pp. 1201-1215, 2000

[19] M. Maute, B. Kögel, G. Böhm, P. Meissner, M.-C. Amann, "MEMS-tunable 1.55 μm VCSEL with extended tuning range incorporating a buried tunnel junction", *IEEE Photon. Technol. Lett.*, vol. 18, no. 5, pp. 688-690, 2006

[20] M. Moser, K.H. Gulden, J. Epler, H.P. Schweizer, "High performance deep red AlAs/AlGaAs top-emitting VCSELs grown by MOVPE at high growth rates", *J. Cryst. Growth*, vol. 170, no. 1-4, pp. 404-407, 1997

[21] M. Moser, Avalon Photonics Ltd., personal communication, 2005

[22] W. Koechner, *Solid-state laser engineering*, Springer-Verlag, 1999, Chapter 2

[23] J. Cruz, G. Giuliani, H.M. van Driel, "Measurement of the subnanosecond, nonradiative relaxation time from excited states of Nd3+ in a Nd:YAG crystal", *Opt. Lett.*, vol. 15, no. 5, pp. 282-284, 1990

[24] Casix Inc.

[25] C. Bibeau, S.A. Payne, H.T. Powell, "Direct measurement of the terminal laser level lifetime in neodymium-doped crystals and glasses", *J. Opt. Soc. Am. B*, vol. 12, no. 10, pp. 1981-1992, 1995

[26] F.T. Arecchi, G.L. Lippi, G.P. Puccioni, J.R. Tredicce, "Deterministic chaos in laser with injected signal", *Opt. Commun.*, vol. 51, no. 5, pp. 308-314, 1984

[27] C.O. Weiss, R. Vilaseca, *Dynamics of Lasers*, VCH Publishers Inc., 1991, Chapter 1

[28] H. Haken, "Analogy between higher instabilities in fluids and lasers", *Phys. Lett. A*, vol. 53, no. 1, pp. 77-78, 1975

[29] Chapter 5, pp. 87-89, in [27].

[30] E.N. Lorenz, " Deterministic nonperiodic flow", *J. Atm. Sci.*, vol. 20, no. 2, pp. 130-141, 1963

[31] J.R. Tredicce, F.T. Arecchi, G.I. Lippi, G.P. Puccioni, "Instabilities in lasers with an injected signal", *J. Opt. Soc. Am. B*, vol. 2, no. 1, pp. 173-183, 1985

[32] C.O. Weiss, W. Klische, P. S. Ering and M. Cooper, "Instabilities and chaos of a single mode NH_3 ring laser", *Opt. Commun*, vol. 52, no. 6, pp. 405-408, 1985

[33] C.O. Weiss, J. Brock, "Evidence for Lorenz-type Chaos in a Laser", *Phys. Rev. Lett.*, vol. 57, no. 22, pp. 2804-2806, 1986

[34] T.B. Simpson, J.M. Liu, "Phase and amplitude characteristics of nearly degenerate four-wave mixing in Fabry-Perot semiconductor lasers", *J. Appl. Phys.*, vol. 73, no. 5, pp. 2587-2589, 1993

[35] J. Ohtsubo, *Semiconductor lasers: stability, instability and chaos*, Springer-Verlag, 2006

[36] K. Petermann, *Laser diode modulation and noise*, Kluwer Academic Publishers, 1991, Chapter VII

[37] G.P. Agrawal, "Spectral hole-burning and gain saturation in semiconductor lasers: Strong-signal theory", *J. Appl. Phys.*, vol. 63, no. 4, pp. 1232-1235, 1988

[38] T.B. Simpson, F. Doft, E. Strzelecka, J.J. Liu, W. Chang, G.J. Simonis, "Gain saturation and the linewidth enhancement factor in semiconductor lasers", *IEEE Photon. Technol. Lett.*, vol. 13, no. 8, pp. 776-778, 2001

[39] L.D. Landau, E.M. Lifshitz, *Electrodynamics of continuous media*, Pergamon Press Ltd., 1960, Chapter IX

[40] M. Lax, "Classical noise V. Noise in self-sustained oscillators", *Phys. Rev.*, vol. 160, pp. 290-307, 1967

[41] M. Lax, "Quantum noise X. Density-matrix treatment of field and population-difference fluctuations", *Phys. Rev.*, vol. 157, pp. 213-231, 1967

[42] G.B. Arfken, H.J. Weber, *Mathematical methods for physicist*, 4th ed., Academic Press, 1995, Chapter 7

[43] M.W. Fleming, A. Mooradian, "Fundamental line broadening of single-mode (GaAl)As diode lasers", *Appl. Phys. Lett.*, vol. 38, pp. 511-513, 1981

[44] C.H. Henry, "Theory of the linewidth of semiconductor lasers", *IEEE J. Quantum Electron.*, vol. QE-18, no. 2, pp. 259-264, 1982

[45] S. Balle, "Effective two-level model with asymmetric gain for laser diodes", *Opt. Commun.*, vol. 119, pp. 227-235, 1995

[46] W.W. Chow, S.W. Koch, M. Sargent III, *Semiconductor-laser physics*, Springer-Verlag, 1997

[47] G.P. Agrawal, C.M. Bowden, "Concept of linewidth enhancement factor in semiconductor lasers: It's usefulness and limitations", *IEEE Photon. Technol. Lett.*, vol. 5, no. 6, pp. 640-642, 1993

[48] J.R. Marciante, P. Agrawal, "Spatio-temporal characteristics of filamentation in broad-area semiconductor lasers", *IEEE J. Quantum Electron.*, vol. 33, no. 7, pp. 1174-1179, 1997

[49] M. Osiński, J. Buus, "Linewidth broadening factor in semiconductor lasers - an overview", *IEEE J. Quantum Electron.*, vol. QE-23, no. 1, pp. 9-29, 1987

[50] European Cooperation in the Field of Scientific and Technical Research. [Online]. Available: http://www.cost.esf.org.

[51] P.G. Drazin, *Nonlinear systems*, Cambridge University Press, 1992

[52] Chapter 5 in [46].

[53] Y. Lien, "Intensity dynamics of slow-inversion lasers", Ph.D. Thesis, Universiteit Leiden, Leiden, The Netherlands, 2002, Chapter 4

[54] M. Willatzen, A. Uskov, J. Mørk, H. Olesen, B. Tromborg, A.-P. Jauho, "Nonlinear gain suppression in semiconductor lasers due to carrier heating", *IEEE Photon. Technol. Lett.*, vol. 3, no. 7, pp. 606-609, 1991

[55] R. Frankenberger, R. Schimpe, "Origin of gain saturation in index-guided InGaAsP laser diodes", *Appl. Phys. Lett*, vol. 60, no. 22, pp. 2720-2722, 1992

[56] F. Girardin, G.-H. Duan, P. Gallion, "Experimental investigation of the relative importance of carrier heating and spectral-hole-burning on nonlinear gain in bulk and strained multi-quantum-well 1.55 μm lasers", *Appl. Phys. Lett.*, vol. 67, no. 6, pp. 771-773, 1995

[57] R.S. Tucker, D.J. Pope, "Circuit modeling of the effect of diffusion on damping in a narrow-stripe semiconductor laser", *IEEE J. Quantum Electron.*, vol. 19, no. 7, pp. 1179-1183, 1983

[58] S. Wieczorek, "The dynamical complexity of optically injected semiconductor lasers", Ph.D. Thesis, Vrije Universiteit, Amsterdam, The Netherlands, 2002, Chapter 2

[59] A.E. Siegman, *Lasers*, University Sciences Books, 1986, Chapter 25

[60] M. Yousefi, D. Lenstra, G. Vemuri, "Carrier inversion noise has important influence on the dynamics of a semiconductor laser", *IEEE Sel. Top. Quantum Electron.*, vol. 10, no. 5, pp. 955-960, 2004

[61] S. Valling, T. Fordell, Å.M. Lindberg, "Experimental and numerical intensity time series of an optically injected solid state laser", *Opt. Commun.*, vol. 254, pp. 282-289, 2005

[62] M.P. van Exter, W.A. Hamel, J.P. Woerdman, B.R.P. Zeijlmans,"Spectral signature of relaxation oscillations in semiconductor lasers", *IEEE J. Quantum Electron.*, vol. 28, no. 6, pp. 1470-1478, 1992

[63] Chapter 5 in [22].

[64] W.A. Hamel, J.P. Woerdman, "Non-orthogonality of the longitudinal eigenmodes of a laser", *Phys. Rev. A*, vol. 40, no. 5, pp. 2785-2787, 1989

[65] K. Petermann, "Calculated spontaneous emission factor for double-heterostructure injection lasers with gain-induced waveguiding", *J. Quantum. Electron.*, vol. 15, no. 7, pp. 566-570, 1979

[66] Z. Toffano, "Investigation of threshold transition in semiconductor lasers", *IEEE J. Sel. Topics Quantum Electron.* vol. 3, no. 2, pp. 485-490, 1997

[67] H. Risken, K. Seybold, "Linewidth of a detuned single mode laser near threshold", *Phys. Lett.*, vol. 38A, pp. 63-64, 1972

[68] R. Hui, S. Benedetto, I. Montrosset, "Near threshold operation of semiconductor lasers and resonant-type laser amplifiers", *IEEE J. Quantum Electron.*, vol. 29, no. 6, pp. 1488-1497, 1993

[69] A. Villafranca, J.A. Lázaro, I. Salinas, I. Garcés, "Measurement of the linewidth enhancement factor in DFB lasers using a high-resolution optical spectrum analyzer", *IEEE Photon. Technol. Lett.*, vol. 17, no. 11, pp. 2268-2270, 2005

[70] Z. Toffano, A. Destrez, C. Birocheau, L. Hassine, "New linewidth enhancement determination method in semiconductor lasers based on spectral analysis above and below threshold", *Electron. Lett.*, vol. 28, no. 1, pp. 9-11, 1992

[71] M.A. Newkirk, K.J. Vahala, "Parasitic-free measurement of the fundamental frequency response of a semiconductor laser by active-layer photomixing", *Appl. Phys. Lett.*, vol. 52, no. 10, pp. 771-773, 1987

[72] K.J. Vahala, M.A. Newkirk, "Parasitic-free modulation of semiconductor lasers", *IEEE J. Quantum Electron.*, vol. 25, no. 6, pp. 1393-1398, 1989

[73] C. Harder, K. Vahala, A. Yariv, "Measurement of the linewidth enhancement factor α of semiconductor lasers", *Appl. Phys. Lett.*, vol. 42, no. 4, pp. 328-330, 1983

[74] R. Schimpe, J.E. Bowers, T.L. Koch, "Characterization of frequency response of 1.5 μm InGaAsP DFB laser diode and InGaAs pin photodiode by heterodyne measurement technique", *Electron. Lett.*, vol. 22, pp. 453-454, 1986

[75] L. Illing, M.B. Kennel, "Shaping current waveforms for direct modulation of semiconductor lasers", *IEEE J. Quantum Electron.*, vol. 40, no. 5, pp. 445-452, 2004

[76] B. Dagens, A. Markus, J.X. Chen. J.-G. Provost, D. Make, O. Le Gouezigou, J. Landreau, A. Fiore, B. Thedrez, "Giant linewidth enhancement factor and purely frequency modulated emission from quantum dot laser", *Electron. Lett.*, vol. 41, no. 6, 2005

[77] S. Melnik, G. Huyet, A. V. Uskov, "The linewidth enhancement factor α of quantum dot semiconductor lasers", *Opt. Express*, vol. 14, no. 7, pp. 2950-2955, 2006

[78] M. Bennett, M.F. Schatz, H. Rockwood, K. Wiesenfeld, "Huygens' clocks", *Proc. R. Soc. Lond.* A, vol. 458, pp. 563-579, 2002

[79] M. Rosenblum, A. Pikovsky, "Synchronization: from pendulum clocks to chaotic lasers and chemical oscillators", *Contemp. Phys.*, vol. 44, no. 5, pp. 401-416, 2003

[80] H.L. Stover, W.H. Steier, "Locking of laser oscillators by light injection", *Appl. Phys. Lett.*, vol. 8, no. 4, pp. 91-93, 1966

[81] R. Adler, "A study of locking phenomena in oscillators", *Proc. IEEE*, vol. 61, pp. 1380-1385, 1973 (reprinted from *Proc. IRE*, vol. 34, pp. 251-357, 1954)

[82] K.T. Alligood, T.D. Sauer, J.A. Yorke, *Chaos: an introduction to dynamical systems*, Springer-Verlag, 2000, Chapter 8

[83] Chapter 7, pp. 273-275, in [82].

[84] K. Ikeda, H. Daido, "Optical turbulence: Chaotic behavior of transmitted light from a ring cavity", *Phys. Rev. Lett*, vol. 45, no. 9, pp. 709-712, 1980

[85] F.T. Arecchi, R. Meucci, G.P. Puccioni, J.R. Tredicce, "Experimental Evidence of Subharmonic Bifurcations, Multistability, and Turbulence in a Q-Switched Gas Laser", *Phys. Rev. Lett*, vol. 49, no. 17-25, pp. 1217-1220, 1982

[86] F.-Y. Lin, J.-M. Liu, "Nonlinear dynamics of a semiconductor laser with delayed negative optoelectronic feedback", *IEEE J. Quantum Electron.*, vol. 39, no. 4, pp. 562-568, 2003

[87] R. Lang, K. Kobayashi, "External optical feedback effects on semiconductor injection laser properties", *IEEE J. Quantum Electron.*, vol. 16, no. 3, pp. 347-355, 1980

[88] R.W. Tkach, A.R. Chrapluvy, "Regimes of feedback effects in 1.5-μm distributed feedback lasers", *IEEE J. Lightwave Technol.*, vol. 4, no. 11, pp. 1655-1661, 1986

[89] G. Giuliani, S. Donati, "Laser interferometry", in: D.M. Kane and K.A. Shore (Eds.), *Unlocking dynamical diversity*, J. Wiley & Sons Ltd, 2005, pp. 217-255

[90] Y. Yu, G. Giuliani, S. Donati, "Measurement of the linewidth enhancement factor of a semiconductor laser based on the optical feedback self-mixing effect", *IEEE Photon. Technol. Lett.*, vol. 16, no. 4, pp. 990-992, 2004

[91] Chapter 7, pp. 248-249, in [46].

[92] J.-M. Liu, T.B. Simpson, "Four wave mixing and optical modulation in a semiconductor laser", *IEEE J. Quantum Electron.*, vol. 30, no. 4, pp. 957-965, 1994

[93] T.B. Simpson, "Mapping the nonlinear dynamics of a distributed feedback semiconductor laser subject to external optical injection", *Opt. Commun.*, vol. 215, pp. 135-151, 2003

[94] R. Hui, A. Meccozi, A. D'Ottavi, P. Spano, "Novel measurement technique of α factor in DFB semiconductor lasers by injection locking", *Electron. Lett.*, vol. 26, no. 14, pp. 997-998, 1990

[95] N.A. Al-Hosiny, I.D. Henning, M.J. Adams, "Correlation of electron density changes with optical frequency shifts in optically injected semiconductor lasers", *IEEE J. Quantum Electron.*, vol. 42, no. 6, pp. 570-580, 2006

[96] G.H.M. van Tartwijk, G. Muijres, D. Lenstra, M.P. Van Exter, J.P. Woerdman, "The semiconductor-laser beyond the locking range of optical-injection", *Electron. Lett.*, vol. 29, no. 2, pp. 137-138, 1993

[97] M.P. van Exter, C. Biever, J.P. Woerdman, "Effect of optical-injection on bias voltage and spectrum of a semiconductor-laser", *IEEE J. Quantum Electron.*, vol. 29, no. 11, pp. 2771-2779, 1993

[98] K.E. Chlouverakis, M.J. Adams, "Stability maps of injection-locked laser diodes using the largest Lyapunov exponent", *Opt. Commmun*, vol. 216, pp. 405-412, 2003

[99] H. Haken, "At least one Lyapunov exponent vanishes if the trajectory of an attractor does not contain a fixed point", *Phys. Lett. A*, vol. 94, no. 2, pp. 71-72, 1983

[100] B. Krauskopf, "Bifurcation analysis of laser systems ", in: B. Krauskopf, D. Lenstra (Eds.), *Fundamental issues of nonlinear laser dynamics: concepts, mathematics, physics and applications*, Vol. 548 of AIP Conference Proceedings, American Institute of Physics, 2000

[101] S. Wieczorek, B. Krauskopf, D. Lenstra, "A unifying view of bifurcations in a semiconductor laser", *Opt. Commun.*, vol. 172, pp. 279-295, 1999

[102] A. Dhooge, W. Govaerts, Y.A. Kuznetsov, *ACM Trans. Math. Softw.*, vol. 29, no. 2, pp. 141-164, 2003

[103] M.K.S. Young, S.H. Strogatz, "Nonlinear dynamics of a solid state laser with injection", *Phys. Rev. E*, vol. 58, no. 4, pp. 4421-4435, 1998

[104] B. Krauskopf, S. Wieczorek, "Accumulating regions of winding periodic orbits in optically driven lasers", *Physica D*, vol. 173, no. 1-2, pp. 97-113, 2002

[105] S. Wieczorek, K. Krauskopf, D. Lenstra, "Unnested islands of period-doublings in an injected semiconductor laser", *Phys. Rev. E*, vol. 64, no. 5, 056204, 2001

[106] Chapter 3, pp. 59-66, in [27].

[107] Chapter 10, pp. 413-417, in [82].

[108] T.B. Simpson, J.M. Liu, A. Gavrielides, V. Kovanis, P.M. Alsnig, "Period-doubling route to chaos in a semiconductor laser subject to optical injection", *Appl. Phys. Lett.*, vol. 64, no. 26, pp. 3541-3543, 1994

[109] S. Wieczorek, T.B. Simpson, B. Krauskopf, D. Lenstra, "Global quantitative predictions of complex laser dynamics", *Phys. Rev. E*, vol. 64, 045207, 2002

[110] T.B. Simpson, J.M. Liu, K.F. Huang, K. Tai, "Nonlinear dynamics induced by external optical injection in semiconductor lasers", *Quantum Semiclass. Opt.*, vol. 9, pp. 765-784, 1997

[111] J.B. Altés, I. Gatare, K. Panajotov, H. Thienpoint, M. Sciamanna, "Mapping of the dynamics induced by orthogonal optical injection in vertical-cavity surface-emitting lasers", *IEEE J. Quantum Electron*, vol. 42, no. 2, pp. 198-207, 2006

[112] S. Eriksson, Å.M. Lindberg, "Observations on the dynamics of semiconductor lasers subjected to external optical injection", *J. Opt. B: Quantum Semiclass. Opt.*, vol. 4, pp. 149-154, 2002

[113] S. Eriksson, "Dependence of the experimental stability diagram of an optically injected semiconductor laser on the laser current", *Opt. Commun.*, vol. 210, no. 3-6, pp. 343-353, 2002

[114] S. Eriksson, Å.M. Lindberg, "Periodic oscillation within the chaotic region in a semiconductor laser subjected to external optical injection", *Opt. Lett.*, vol. 26, no. 3, pp. 142-144, 2001

[115] T. Fordell, Å.M. Lindberg, B. Ståhlberg, "Dynamics of an optically injected semiconductor laser near 690 nm", *Northern Optics*, Espoo, Finland, 2003

[116] P.M. Boers, M.T. Vlaardingerbroek, M. Danielsen, "Dynamic behaviour of semiconductor lasers", *Electron. Lett.*, vol. 11, no. 10, pp. 206-208, 1975

[117] C.-H. Lee, T.-H. Yoon, S.-Y. Shin, "Period doubling and chaos in a directly modulated laser diode", *Appl. Phys. Lett*, vol. 46, no. 1, pp. 95-97, 1985

[118] C. Szwaj, E. Lacot, O. Hugon, "Large linewidth-enhancement factor in a microchip laser", *Phys. Rev. A*, vol. 70, 033809, 2004

[119] T.-S. Lim, T.-H. Yang, J.-L. Chern, K. Otsuka, "Phase-noise driven instability in a single-mode microchip Nd:YVO_4 laser with feedback", *IEEE J. Quantum Electron.*, vol. 37, no. 9, pp. 1215-1225, 2001

[120] S. Valling, B. Krauskopf, T. Fordell, Å.M. Lindberg, "Experimental bifurcation diagram of a solid-state laser with optical injection", *Opt. Commun.*, vol. 271, no. 2, pp. 532-542, 2007

[121] M. Vainio, M. Merimaa, K. Nyholm, "Optical amplifier for femtosecond frequency comb measurements near 633 nm", *Appl. Phys. B*, vol. 81, no. 8, pp. 1053-1057, 2005

[122] T.B. Simpson, J.M. Liu, "Bandwidth enhancement and broadband noise reduction in injection-locked semiconductor lasers", *IEEE Photon. Technol. Lett.*, vol. 7, no. 7, pp. 709-711, 1995

[123] L. Chrostowski, X. Zhao, C.J. Chang-Hasnain, R. Shau, M. Ortsiefer, M.-C. Amann, "50-GHz Optically injection-locked 1.55 μm VCSELs", *IEEE Photon. Technol. Lett.*, vol. 18, no. 2, pp. 367-369, 2006

[124] P.C. Peng, Y.H. Chang, H.C. Kuo, W.K. Tsai, G. Lin, C.T. Lin, H.C. Yu, H.P. Yang, R.S. Hsiao, K.F. Lin, J.Y. Chi, S. Chi, S.C. Wang, "1.3 μm quantum dot vertical-cavity surface-emitting laser with external light injection", *Electron. Lett.*, vol. 41, no. 22, 2005

[125] S. Wieczorek, W.W. Chow, L. Chrostowski, C.J. Chang-Hasnain, "Improved semiconductor-laser dynamics from induced population pulsation", *IEEE J. Quantum Electron.*, vol. 42, no. 6, pp. 552-562, 2006

[126] T.B. Simpson, F. Doft, "Double-locked laser diode for microwave photonics applications", *IEEE Photon. Technol. Lett.*, vol. 11, no. 11, pp. 1476-1478, 1999

[127] S.-C. Chan, J.-M. Liu, "Frequency modulation on single sideband using controlled dynamics of an optically injected semiconductor laser", *IEEE J. Quantum Electron.*, vol. 42, no. 7, pp. 699-705, 2006

[128] S.-C. Chan, J.-M. Liu, "Microwave frequency division and multiplication using an optically injected semiconductor laser", *IEEE J. Quantum Electron.*, vol. 41 , no. 9, pp. 1141-1147, 2005

[129] J. Ohtsubo, P. Davis, "Chaotic optical communication", in: D.M. Kane and K.A. Shore (Eds.), *Unlocking dynamical diversity*, J. Wiley & Sons, 2005

[130] I. Fischer, Y. Liu, P. Davis, "Synchronization of chaotic semiconductor laser dynamics on subnanosecond time scales and its potential for chaos communications", *Phys. Rev. A*, vol. 62, 011801(R), 2000

[131] P. Colet, R. Roy, "Digital communication with synchronized chaotic lasers", *Opt. Lett.*, vol. 19, pp. 2056-2058, 1994

[132] V. Annovazzi-Lodi, M. Benedetti, S. Merlo, M. Norgia, B. Provinzano, "Optical chaos masking of video signals", *IEEE Photon. Technol. Lett.*, vol. 17, no. 9, pp. 1995-1997, 2005

[133] F.Y. Lin, J.-M. Liu, "Chaotic radar using nonlinear laser dynamics", *IEEE J. Quantum Electron.*, vol. 40, no. 6, pp. 815-820, 2004

[134] H. Yoo, Y.D. Jeong, Y.H. Won, M. Kang, H.J. Lee, "All-optical wavelength conversion using aborption modulation of an injection-locked Fabry-Pérot laser diode", *IEEE Photon. Technol. Lett.*, vol. 16, no. 2, pp. 536-538, 2004

[135] Y. Yang, Y.J. Wen, A. Nirmalathas, H.F. Liu, D. Novak, "Optical clock recovery at line rates via injection locking of a long cavity Fabry-Pérot laser diode", *IEEE Photon. Technol. Lett.*, vol. 16, no. 6, pp. 1561-1563, 2004

[136] A.C. Bordonalli, C. Walton, A.J. Seeds, "High-performance phase locking of wide linewidth semiconductor lasers by combined use of optical injection locking and optical phase-lock loop", *IEEE J. Lightwave Technol.*, vol. 17, no. 2, pp. 328-342, 1999

[137] Chapter 3 in [53].